

McGill Rocket Team Project Stella II

Team 93 Project Technical Report for the 2018 IREC

Jonathan Lesage*, Sandro Papais†, Charles Cossette‡, Liem Dam-Quang§, Daniil Lisus¶, Ksenia Kolosova||, Julien Otis-Laperriere**
McGill University, Montreal, Quebec, H3A 0E9, Canada

This document presents McGill University’s 30,000 ft COTS Motor Category rocket, *Stella II*. It is the successor to an earlier version, which had a flight in IREC 2017. *Stella II* features a radically improved airframe, simplified recovery system, triple-redundant tracking systems, and significantly more student-made components; all of which have been validated by rigorous testing.

I. Introduction

The 2018 IREC marks McGill’s 4th year participating in the competition. The McGill Rocket Team has grown substantially in the past year, owing to the increased interest in aerospace engineering and space exploration at McGill, and now has over 120 members divided amongst Propulsion, Payload, Aerostructures, Recovery and Management divisions. *Stella II* is the successor to *Stella*, the team’s first 30,000 ft COTS category entry. Following the off-nominal flight of *Stella* last year, the team has fundamentally reworked the recovery system design and airframe manufacturing process to prevent the same issues from reoccurring. To further validate the changes, the team has built a secondary rocket, *Bertrand*, which will fly on a test launch on June 2ndnd, 2018. However, manufacturing an entirely separate rocket to test critical recovery and avionic systems increased financial costs. In order to help offset the additional costs, the group expanded the number of student-made components, replacing off-the-shelf pieces. Only 3 of the 53 major components in *Stella II* were off-the-shelf - being the motor itself, the avionic redundancy, and a motor retaining ring. Student made components such as parachutes, shock cords, CO2 ejectors, tender-descenders, and the airframe lead to cost savings of several thousand dollars.



Figure 1 *Stella II*'s external geometry and appearance.

II. System Architecture Overview

Stella II is divided into four main subsystems: propulsion, aero-structures, recovery and payload. The propulsion unit is an O-class Cesaroni motor. The aero-structure subsystem features a composite airframe manufactured in-house using a refined resin infusion process. This method was perfected over the course of the year and allows for high quality, tight dimensional tolerance composite structures as well as reduced lead times.

The avionics are centralized in a radio-transparent fiberglass airframe section, featuring triple-redundant ejection and telemetric systems. The centralized avionic section allows for rapid, convenient assembly, and easy access to the ejection charges located in the forward parachute chamber. A single separation point is located at the nose cone, which

*Team Captain, McGill Rocket Team.

†Team Captain, McGill Rocket Team.

‡Been here for way too long, McGill Rocket Team.

§Propulsion Division Lead, McGill Rocket Team.

¶Payload Division Lead, McGill Rocket Team.

||Payload Division Lead, McGill Rocket Team.

**Propulsion Division Member, McGill Rocket Team.



Figure 2 *Stella II's* internal configuration.

houses a payload intended to measure the pressure distribution on the cranial cavity resulting from high accelerations. <https://preview.overleaf.com/public/pnshnvtcvwyw/images/a4c619f8320208016b5056cec53ecb90fe978426.png>

Table 1 Key Technical Specifications

Specification	Value	Target	Units
Airframe Length	11	-	feet
Airframe Diameter	5.00	5.00±0.01	inches
Liftoff Mass	74.5	<75	lbm
Peak Thrust	1067.9	-	lbf
Max Mach Number	1.72	-	-
Motor	Cesaroni O3400	-	-
Predicted Apogee	31,047	30,000	feet
Thrust/Weight Ratio	10.3	>5	-
Rail Departure Speed	119	>100	feet/second
Minimum Static Margin	1.65	>1.5	calibers
Maximum Static Margin	5.74	<6	calibers

A. Propulsion subsystems

Stella II employs a Cesaroni Pro98 O3400-P, with a total impulse of 21,062 Ns over 6.16s. This motor provides sufficient force to reach the required off-the-rod velocity, and the impulse to reach the target altitude of 30,000 ft. *Stella II's* flight behavior was simulated using OpenRocket, an open-source rocketry simulation tool [1]. The simulation parameters attempt to match the Spaceport America conditions as closely as possible given available information. Simulation wind speed was set as 7.18 mph, the average of morning (9am) wind speeds over the last 14 days of June 2017 measured in Truth or Consequences, NM [2]. Ground level altitude was set to 4600 ft, and the launch rail was set to a length of 17 ft at an angle of 6° from vertical.

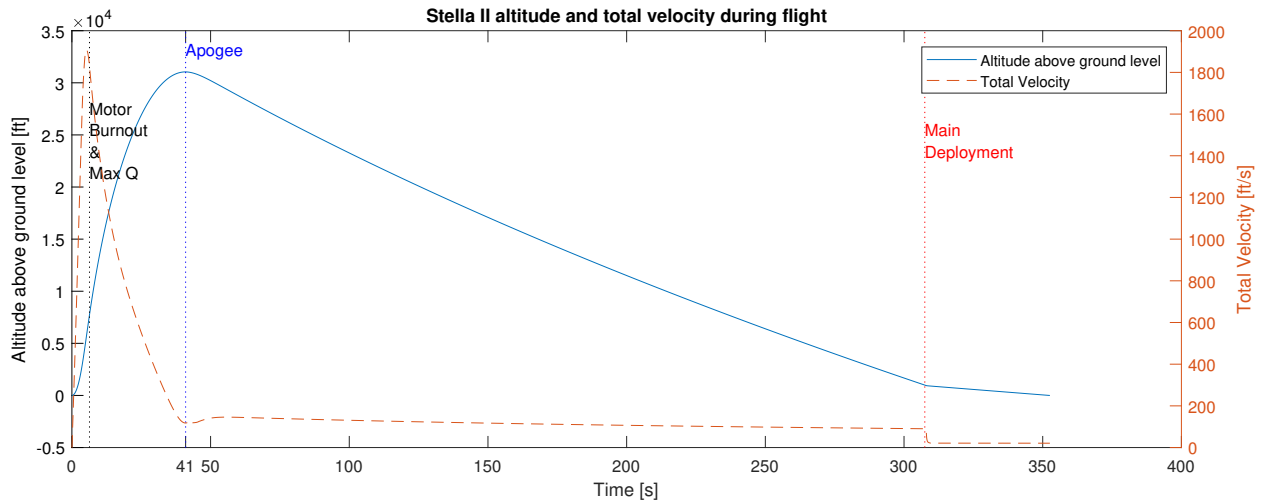


Figure 3 *Stella II* above ground altitude and total velocity during flight, with key flight events marked.

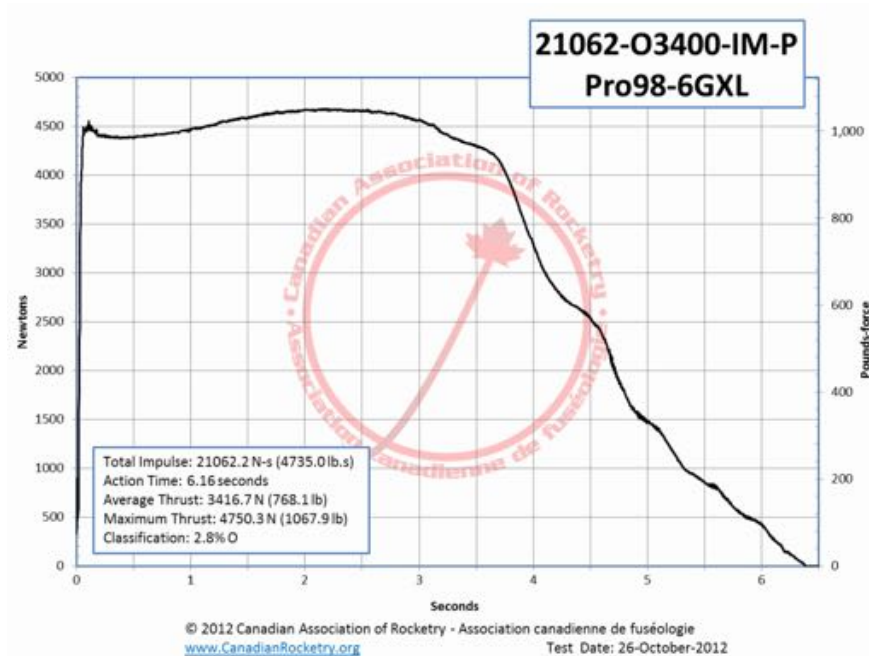


Figure 4 Thrust curve of COTS O3400 motor.

Other flight metrics of interest were three dimensionless coefficients: the stability margin, Mach number, and thrust-to-weight ratio, which are plotted in Figure 5. The position of the center of pressure on the rocket varies during because of variations in the orientation of the rocket, as well as variations in the pressure field around the rocket. The Mach number of a moving aircraft is the ratio between its speed and the speed of sound in the surrounding atmosphere, while the thrust to weight ratio is the ratio between instantaneous motor thrust and the weight of the rocket. The latter decreases as the motor burns.

During flight, the air around the rocket also exerts pressure and drag on the airframe. To compute the dynamic air pressure on the rocket, the compressibility of air has to be taken into account. Assuming an isentropic flow (where skin friction does not significantly heat up the flow), the ratio of total pressure to static pressure is given by

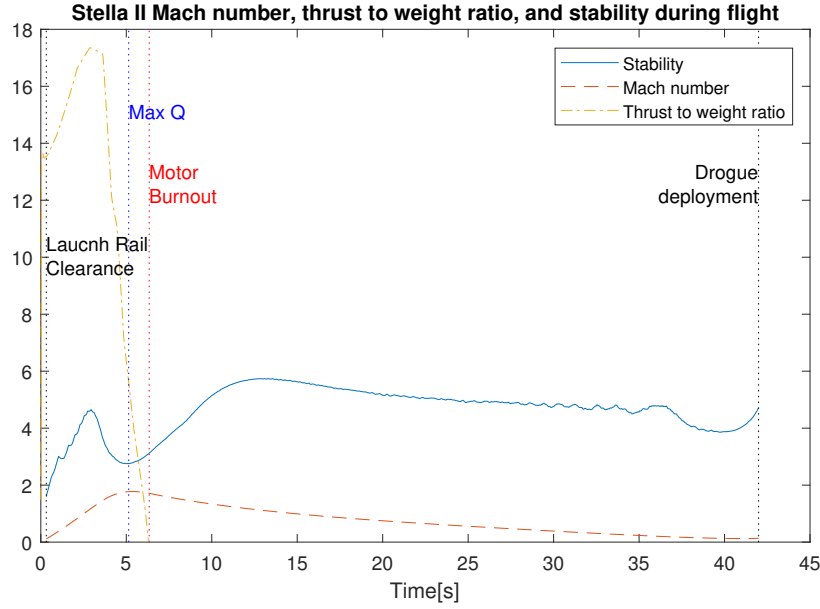


Figure 5 *Stella II* dimensionless metrics during flight.

$$\frac{P_t}{P} = \left(1 + \frac{\gamma - 1}{2} M^2\right)^{\frac{\gamma}{\gamma - 1}}$$

where P_t is the total pressure, P is static pressure, γ is the specific heat ratio and M is the Mach number [3]. Assuming that $\gamma = 1.400$, and given that $P_t = P + q_c$, the compressive dynamic pressure, q_c , is given by

$$q_c = P \left[\left(1 + 0.2M^2\right)^{\frac{7}{2}} - 1 \right].$$

Note that the static pressure is determined by OpenRocket using an International Standard Atmosphere model, and values from this model are used in calculations. The drag force shown in Figure 6 is also calculated directly by OpenRocket.

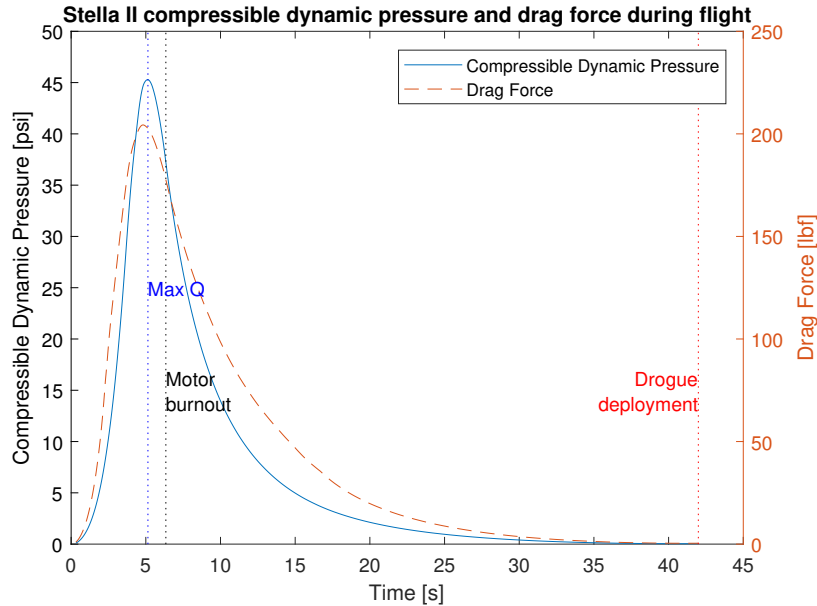


Figure 6 *Stella II* dynamic pressure and drag force during flight

The large force applied to the airframe from the motor called for the use of a carefully designed set of engine blocks. These prevent the motor from ripping through the rocket during peak thrust. *Stella II's* engine block system consists of a top and bottom piece. The bottom piece acts as a mounting point for the motor, while the top acts to prevent failure of the COTS retaining ring and is a mounting point for the avionics.

These components are manufactured from 6061-T6 Aluminum. This provides a lightweight solution to the engine block, while also maintaining a reasonable level of strength. A finite element analysis shown in Figure 7 was completed on both components with realistic loading scenarios. Using the ANSYS static structural module, the bottom engine block had a safety factor of 2, while the top had one of 1.3. Both blocks are capable of withstanding the full load alone, and together they provide more than the necessary amount of support for the motor.

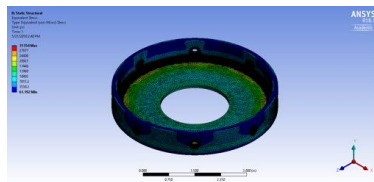


Figure 7 Top engine block under maximum expected load.

B. Aero-structures subsystems

Stella II features an entirely composite SRAD airframe. This airframe consists of primarily carbon fiber reinforced polymers (CFRP), with some glass fiber reinforced polymer (GFRP) components. The airframe built upon many of the lessons learned from *Stella*, leading to the expansion and refinement of the vacuum assisted resin infusion (VARI) process. This approach led to significant weight savings, improved tolerances, reduced production times, and increased member involvement.

The new design seeks to address many of the issues identified in the airframe of *Stella*. The off-nominal flight experienced was attributed to a failure in the airframe of some form. Several possible causes for this exist, including an avionics bay access panel failure, fin de-lamination, misalignment of body tubes and couplers, structural failure due to excessive bending moments, and over-stability. In this iteration of *Stella*, the access panel has been completely removed and the frame is completely closed off. The fins are solid 0.25" thick carbon fiber plates, which are further reinforced at

the root. The design is also 18" shorter than before, reducing bending moments and preventing over-stability. Finally, the new mold design greatly improved the tolerances, drastically reducing misalignment problems.

1. Overview of VARI Processes

All composite components of the airframe were manufactured using a VARI process. VARI processes function by using atmospheric pressure to push the resin through a dry pre-form. This process is displayed at three stages for a flat plate in Figure 8. The first stage shows the compacted pre-form with consumables on tool. The second stage shows a snapshot of the resin traveling through the part, impregnating it. Finally, in the third stage the composite cures under vacuum pressure. The process greatly limits the manufacturing time compared to wet layup techniques, and also eliminates the need for high cost equipment such as ovens or autoclaves required with pre-impregnated materials. At the same time, it provides a reasonable fiber volume fraction, suitable for the purposes of the team.

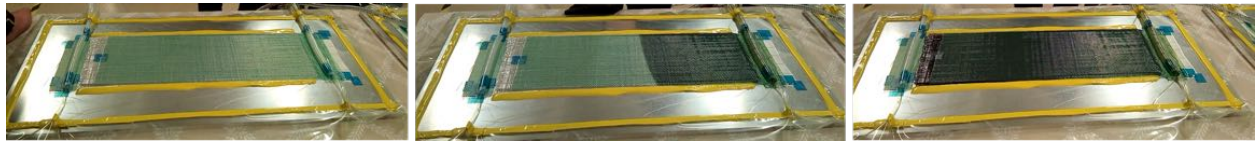


Figure 8 Overview of the VARI process employed on a flat plate.

This process was introduced in *Stella*, where it was employed to create the body tubes. *Stella II* sees an expansion and significant refinement of the process. This led to improved tolerances, eliminated de-lamination issues, and provided an excellent surface finish. No composite component in *Stella II* is COTS.

2. Nose Cone

Stella II's nose cone is a von Karman type cone, manufactured with CFRP. The shape was selected in order to minimize pressure drag during the subsonic regime of the flight. Additionally, simulations in OpenRocket showed that such a geometry was acceptable for travel to the target altitude.



(a) von Karman CFRP nose cone design.

(b) Internal nose cone assembly, showing payload housing.

Figure 9 *Stella II's* nose cone design.

The CFRP construction consists of a non-crimp cross-ply fabric. The stitched fabric was deliberately chosen for its workability during the layup. Compared to woven dry fabrics, stitched fabrics have proven far easier to manage for the team during manufacturing. Additionally, stitched fabrics display improved mechanical properties compared to woven ones, as the fibers are not deformed by the weave. Finally, CFRP was chosen over GFRP due to the significant weight reduction found with carbon fibers. Carbon fibers have a density of 0.065 lbm/in^3 , while common glass fibers have one of 0.090 lbm/in^3 .



Figure 10 Renshape nose cone molds after finishing.

The nose cone has an aluminum tip at the front. This permits better system integration with the payload, which is housed in the nose cone, and presents a simple solution to creating the sharp tip.

For the first time, this component was manufactured using VARI. Its mold, pictured in Figure 10, was machined out of a modeling board called *Renshape* on a CNC router. This ensured a high degree of precision during manufacturing. Afterwards, a polyester mold coating was applied to the surface, followed by sanding and buffing to a mirror-like finish. This ensured an excellent surface finish on the final component.

After several attempts, the component was successfully manufactured using fiberglass and vinylester resin. This led to the manufacturing of the final component in CFRP, shown in Figure 11. The part displayed good tolerances, effectively mating with couplers and body tubes.



Figure 11 Completed CFRP nose cone

3. Body Tubes and Couplers

Stella II's body tubes and couplers feature a mix of CFRP and GFRP parts. GFRP was placed in areas where radio frequency transparency was required. Outside of these areas, CFRPs were used exclusively. This maximized strength in

local areas, and provided increased weight savings compared to its GFRP counterparts. As an example, a CFRP coupler weighed 0.6 lbs less than a GFRP coupler of equivalent length.

The selection of fiber angle was based on considerations of compressive loads, buckling limits, and bending moments in flight. In some scenarios, fiber angle was chosen based on available material. However, orthotropic analysis based on Hashin, quadratic, and maximum stress failure criteria showed excessive safety factors in all components, giving significant confidence in the design of the structure.

CFRP body tubes and couplers feature a $[\pm 28, 0, 0]_s$ layup. These angles have an equivalent stiffness of 12.8 MSI, and bending stiffness of 90.8 Glb-in. This displays an increase of 88% in equivalent stiffness and an increase of 90% in bending stiffness compared to the previous quasi-isotropic layup employed in *Stella*.

GFRP body tubes feature a cross-ply $([0,90])$ layup. This selection was dictated by the material available to the team, and appeared to be the best compromise available. Similarly, the GFRP coupler of the avionics bay is of $[\pm 45]$ degree layup due to available material. These layups show some reduction in properties compared to the layup of the CFRP components, however, these too show excessive safety factors, and as such do not pose concerns for the integrity of the airframe.

When available, as in the case with all CFRP components and the avionics bay, braided or stitched tubular preforms were employed. This minimized layup time, permitting layup times of 45 minutes for full length body tubes. This is a significant reduction in layup time compared to 90 minutes with sheet fabrics. However, the sheet and spray adhesive approach was still employed for the GFRP body tube.

As the body tubes of *Stella* were manufactured using VARI, the process was only improved for *Stella II*, and expanded to the couplers. Rather than employing a GFRP mold, Renshape molds were machined on a CNC router and then coated with polyester, as completed with the nose cone mold. This produced similar results to the nose cone in final part quality, as seen in Figure 12.



(a) Renshape molds after machining and coating.



(b) Body tube after removal from the mold.



(c) Coupler fit with no sanding.

Figure 12 Body tube mold and manufacturing results.

In an attempt to better understand the manufacturing process, VARI was simulated within PAM-RTM. After characterizing the fiber volume fraction at one atmosphere of pressure, and the permeability of the CFRP body tube preform, a simple simulation was created as in Figure 13. This showed the fill time to be 16 minutes, well below the 60 minute gel time of the resin system.

This approach, when applied properly, displayed excellent results. The body tubes were within 0.01" of their target dimension, and showed a very consistent mass. Of all the body tubes produced, a mass of 4.40 lbs \pm 0.06 lbs was

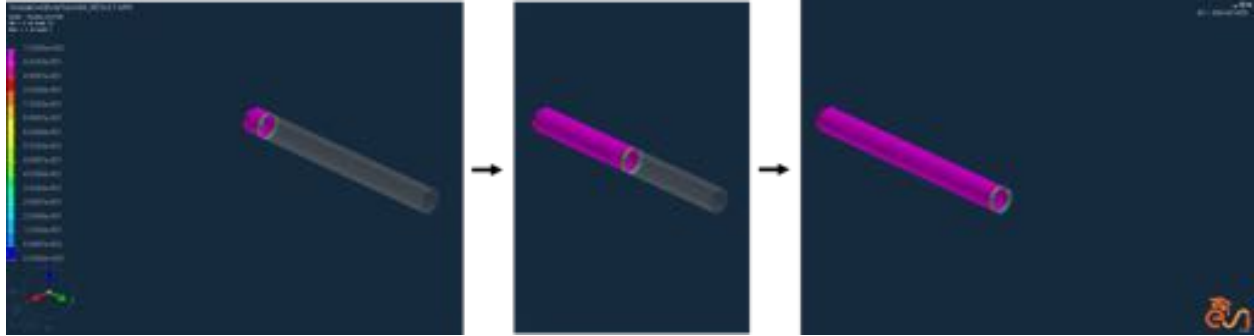


Figure 13 Infusion simulation results at 6, 239, and 899 seconds.

observed when at a length of 48". This demonstrates a consistent manufacturing quality amongst the parts. Similar dimensional results were obtained with the couplers, allowing for a tight fit directly out of the mould into the body tubes.

Some testing took place on the CFRP tubes. An attempt was made to cause failure in the tube under compressive loading. The final part failed after 21,264 lbs, well above the maximum expected loads. However, this only induced failure on part of the tube, likely due to a non-square end of the tube. The failed part is shown in Figure 14.



Figure 14 Failed body tube sample after compressive testing.

4. Fins

The fins of *Stella II* are made exclusively of the same non-crimp fabric as the nose cone. However, these are oriented in a $[(0/90)_2, (\pm 45)_2, (0/90)]_s$ layup. This attempts to achieve a quasi-isotropic layup, one where the stiffness is equal in all directions, to better resist normal and torsional bending moments experienced in flight.

The primary failure mode of the fins for this component is flutter, or divergence. As such, great care was taken in order to ensure the fin was of the proper thickness. The most critical moment for the fin occurs at maximum dynamic pressure, coincident with peak velocity. Using the predicted atmospheric conditions at this point from OpenRocket, the flutter and divergence Mach numbers were calculated in AeroFinSim using the U-G method. This showed that with the actual fin thickness of 0.235", the flutter Mach number was 2.83. This is beyond the maximum velocity of flight, Mach 1.72, giving a fair margin for the fins.

As the fins have the largest influence on the centre of pressure, they have significant influence on the stability in

flight. The geometry of a trapezoidal fin was chosen to ensure greater resistance to flutter, but refined to maintain stability within the required range. Simulations from OpenRocket, displayed in Figure 15, show that the stability off the rod is near 1.5 calibers, and never exceeds 6.0 calibers.

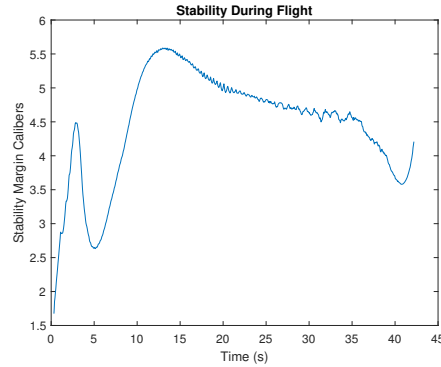
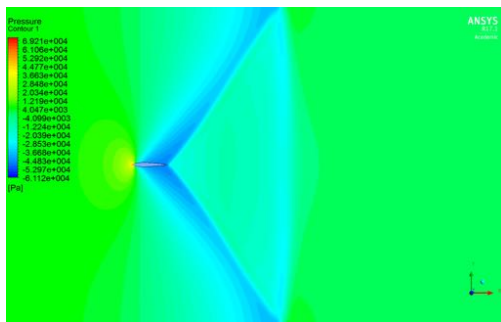


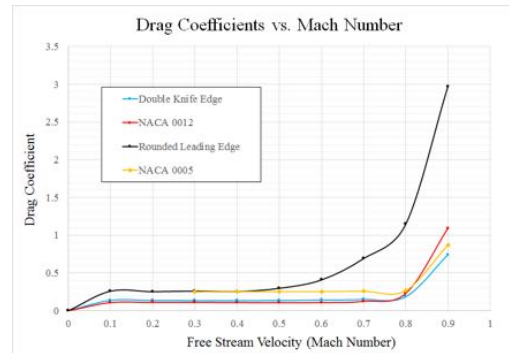
Figure 15 Stability evolution during flight.

These fins are attached with a through-the-wall design. Unlike previous years, the fins are mounted by gluing them into a slot. Afterwards, the fins were given a fillet at the root chord and reinforced with additional CFRP in the region. This ensured that the most likely location of failure would be given sufficient reinforcement for in-flight loading.

The fins feature a double knife edge cross section. After having completed a study using computational fluid dynamics in the subsonic regime, it was shown that minimal performance losses would be incurred by using this shape over that of an airfoil. Additionally, this study showed that in the transonic regime, the double knife edge greatly outperformed the airfoil, as seen in Figure 16. As such, due to its manufacturing simplicity and acceptable performance, the shape was chosen.



(a) Shockwave formation over a NACA0012 airfoil at $M=0.9$, a principal consideration against the use of airfoils for supersonic flight.



(b) Drag coefficients of various cross sections found using CFD.

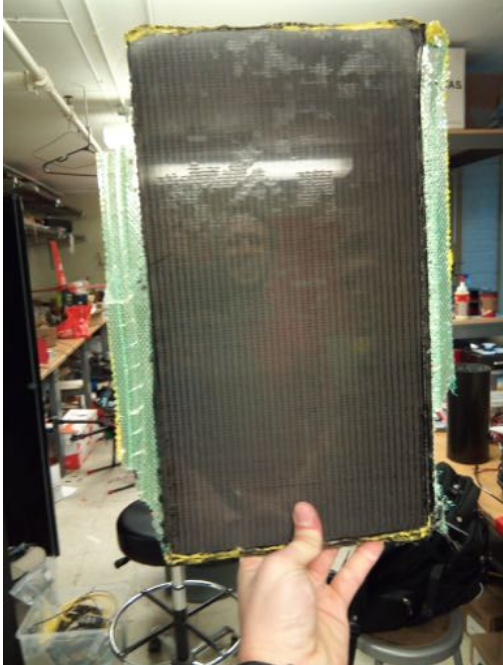
Figure 16 Fin CFD results.

The fins displayed a different manufacturing challenge compared to the other components. The primary goal was to successfully make a component with two tool sides. That is, to create two smooth flat surfaces. As the fin was relatively small, a pseudo-RTM process was applied as seen in Figure 17. This forced the resin directly through the preform, which resulted in a flat plate of consistent thickness, which could later be machined. The consequence of this, however, was a large increase in fill time compared to other parts.

Machining the fins and placing them in the body tubes accurately was of the utmost importance. To achieve the required tolerance, several jigs were manufactured on the CNC router from medium-density fiberboard (MDF). This included a fin cutting jig, a body tube slotting jig, and a fin alignment jig, displayed in Figure 18. A hand-



(a) Compressed fin preform under aluminum caul plate.



(b) Fin plate stock after de-molding.

Figure 17 Fin manufacturing methodology.

held router with a carbon fiber mill would follow these guides, accurately making the cuts in the CFRP part.



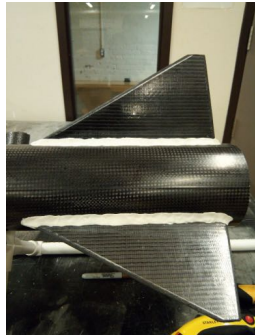
(a) Student made fin-slottting jig. Small human for scale.



(b) Hand-held Router Cutting template for the fins.

Figure 18 Three jigs used in the machining and installation of the fins.

The final step of the fin manufacturing was to attach them to the body tube. This consisted of a three-step process, depicted in Figure 19. First, the fins were attached using epoxy, followed by the addition of an epoxy clay fillet. Afterwards, the root chord was reinforced with additional CFRP using wet lay-up techniques. Additional finishing work, including sanding and filler, was required afterwards.



(a) Attached fin with epoxy clay fillet.



(b) Reinforcement under vacuum bag.



(c) Reinforced fins before finishing operations.

Figure 19 Fin reinforcement procedure.

C. Recovery subsystems

Reliability was the principal consideration during the design of the recovery system. The team deemed a simple, traditional recovery deployment method to be the approach that would maximize the probability of successful parachute inflation. The recovery mechanism features a single-separation, dual-deployment sequence which can be seen in Figure 20.

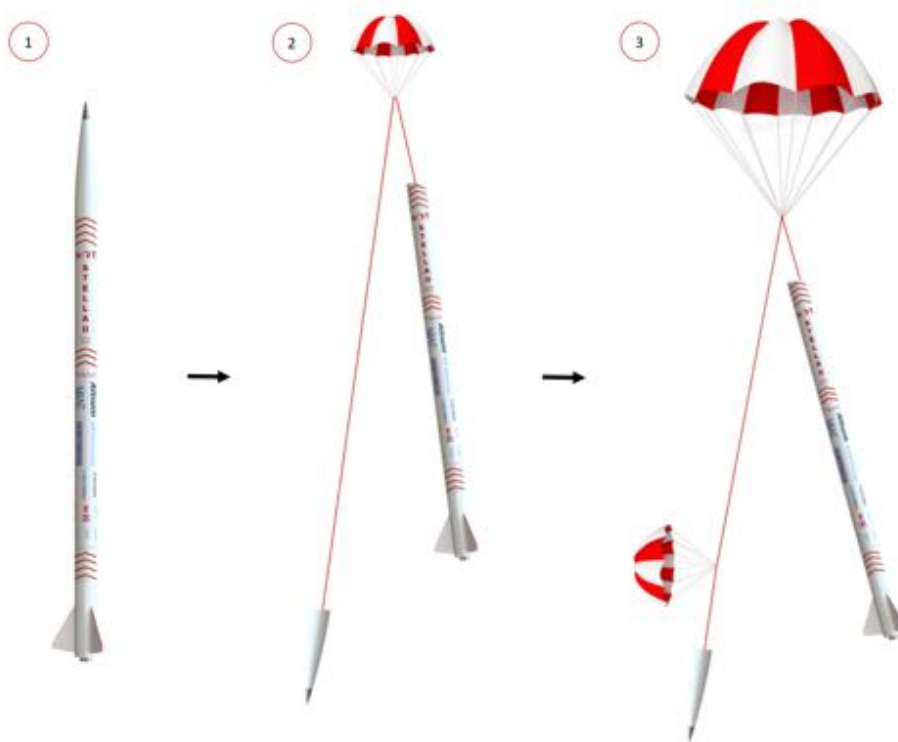


Figure 20 High-level recovery sequencing; including ascent, drogue descent, and main descent phases.

Table 2 Results of ejection tests.

Test #	Description	BP Quantity [g]	# of Shear Pins	Result
1	Empty parachute chamber	2.0	2	Success
2	Full parachute chamber	2.0	2	Failed
3	Relocated charge wells	2.0	2	Failed
4	Added spacing bulkhead	2.0	2	Success
5	Increased Shear pins	3.0	4	Success
6	Full deployment sequencing	3.0	4	Success
7	Full deployment sequencing	3.0	4	Success

1. Parachute Deployment System

The traditional black powder-based separation mechanism is implemented to create an opening in the airframe. Three grams of FFFFg black powder are used to reliably eject the nose cone, which is retained by 4 nylon shear pins, with a safety factor of 1.6 and a second redundant charge. Acknowledging that the air pressure near 30,000 ft is only 26% of that at ground level, the black powder charge wells are a sealed air-tight container with sufficient volume to ensure that the black powder has enough air to ignite properly at apogee. Ground tests of the ejection were repeatedly performed until consistent ejection was achieved; the results of which can be viewed in Table 2.



(a) Ejection test setup.



(b) Successful ejection.

Figure 21 Sample successful nose cone separation test.

As a redundant system, a student-designed CO₂ Ejection system is implemented, and intended to work in parallel with the air-tight black powder charge. Either of these mechanisms are theoretically sufficient to separate the nose cone. The CO₂ ejection mechanism and its successful release of CO₂ can be viewed in Figure 22.

The ejection momentum of the nose cone pulls open the nomex-protected drogue chute, and the drogue descent phase begins. The main parachute is restrained within the tube by a student-designed version of a *tender descender*, which is a breakable link broken by a separate black powder charge at the desired main parachute deployment altitude of 1000 ft. A SRAD tender descender may be viewed in Figure 23.



(a) Loaded with 45g CO2 cannisters.



(b) Successful puncturing of 16g cannister.

Figure 22 Student designed CO2 puncturing device.



(a) Separation force test.



(b) Black powder separation test.

Figure 23 Student-designed tender descender.

The tender descenders were experimentally verified to require 35 lbs of force for separation, which 0.08 grams of black powder can achieve with a safety factor of 3.4. Both parachutes of *Stella II* were designed and manufactured by

students on the team. To prevent tangling during main parachute deployment, the drogue parachute lines are protected by a permeable mesh, as seen in Figure 24. This mesh is capable of allowing sufficient air flow to inflate the drogue parachute, yet prevent any parachute lines from tangling.



(a) Inflated drogue parachute with mesh.



(b) Inflated main parachute.

Figure 24 Student-fabricated parachutes.

The drogue and the main parachutes share the same design, only at different scales. Respectively, the drogue and main consist of 8 and 12 gores, measure 24 inches and 108 inches in open area diameter, and allow for a terminal descent speed of 95 ft/s and 21 ft/s. The coefficient of drag of the design is estimated to be approximately 1.5. Their cross-section resembles a semi-ellipsoid with a flattened-top. This allows for a smaller amount of canopy fabric to be used for a given diameter, therefore reducing packing volume and mass compared to the traditional half-dome shape. Fabric-savings from using this shape gives rise to a trade-off with the coefficient of drag, but it is minimal when compared to that of diameter reduction. Additionally, a vent hole at the top of the canopy, occupying 3% of the open area of the parachute, is integrated for better stability.

Both the drogue and the main parachutes are manufactured using the same technique, but the drogue is further affixed with a mesh overlay to prevent line tangling. All gores are stitched together using a flat-felled seam, chosen for its strength and neatness. Shroud lines are triple-stitched to the canopy with grograin ribbon. The parts of the parachute which undergo the largest amount of stress, the vent hole and the shroud line attachment points, are further reinforced using bias tape and bartacks respectively. The shroud lines measure 1.15 times the diameter of the parachute, while the attachment point lengths measure 10% of it. All stitching is done using coated nylon thread. The canopy fabric is composed of 1.1 oz calendered nylon, where its surface is specially treated for very low porosity. The shroud lines consist of #400 nylon (rated at 400 lb strength) which are made of 8 inner strands contained within an outer sheath. The base of the shroud lines is looped around a small piece of shock cord attached to a 2000 lb-rated M8 swivel.

The deployment bags and blankets are made using a fabric composed of a nomex and kevlar blend, which are both fire-retardant. The drogue parachute is folded and wrapped with a flat piece of that fabric so that it can freely deploy, while the main parachute is contained within a deployment bag. The bag is in a cylindrical shape with a diameter slightly smaller than that of the body tube so that it can slide out smoothly. Rows of sectioned elastic bands are integrated into the bag, so that shroud lines may be packed and secured for a controlled deployment. Furthermore, cylindrical protective sheaths for tender descenders are also made using the same material. Finally, shock cords are created using 1

inch wide stock tubular nylon webbing cut to size with 1-inch loops with 5-inch folds are sewn at both ends.

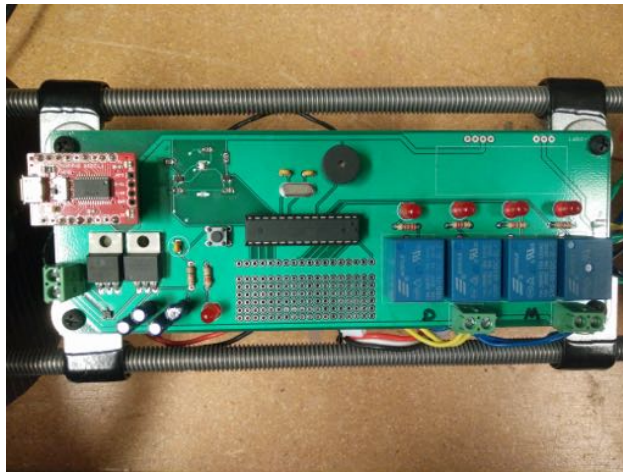
2. Avionics

Blanche's avionics modules are organized into four separate modules, outlined in Table 3. All of these modules are independent, and are powered by separate batteries. This independence was implemented to ensure other modules would continue functioning if one were to fail due to power issues. Furthermore, independent systems allowed more member involvement.

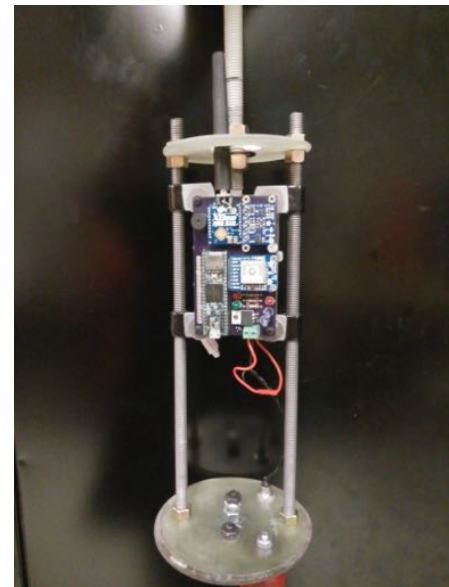
Table 3 Summary of avionics modules.

Module Name	Description	Type	Expected Life	Transmission Frequency
Ejection	Barometer-based parachute deployment	SRAD	16 hours	N/A
Telemetry	Flight data and diagnostic transmission	SRAD	15 hours	902 MHz
RF Beacon	Direction finding beacon	SRAD	46 hours	145 MHz
AIM XTRA	Ejection and Telemetry redundancy	COTS	12 hours	433 MHz

The principle SRAD ejection circuit is kept simple; barometer measurements are filtered by a 1st-order low-pass filter, to give an altitude estimate. The altitude estimate allows apogee detection, which in-turn triggers electromechanical relays. Two relays are inserted in series to prevent accidental e-match firing if one of the relays is accidentally activated (through high accelerations, software bugs, etc). The above is implemented on the ATMEGA328P, and can be viewed in Figure 25



(a) Ejection circuit.



(b) Telemetry, diagnostics, and datalogging circuit.

Figure 25 SRAD circuits.

A SRAD telemetry module was also designed. Transmitting using a pair of XBEE Radios on 900 MHz, this module is capable of sending GPS Coordinates, altitude, battery voltages, internal temperatures, and velocity in real time. The student-designed ground station is designed to be easily portable, and outfitted with a high-gain antenna for enhanced signal reception. Even more data, such as inertial and magnetic measurements, are recorded on an SD Card.

As a second redundancy for recovering the rocket, the team implemented a simple Radio Beacon. An amateur radio license was obtained in order to access the transmission frequencies, and the callsign is included in the Morse-Code message that the beacon emits, “VE2COR MCGILL”. This module was intended to have an outstanding battery life, in the event that the recovery team fails to find a landed rocket on the launch day. Given the 46-hour battery life, the team may still have a chance of locating the rocket using the direction-finding method. By using a 7-element yagi antenna and a software defined radio, the team can seek the direction of strongest signal. Furthermore, this module can be configured to communicate with the telemetry module, and re-broadcast the GPS coordinates on this frequency using the AX.25 protocol.

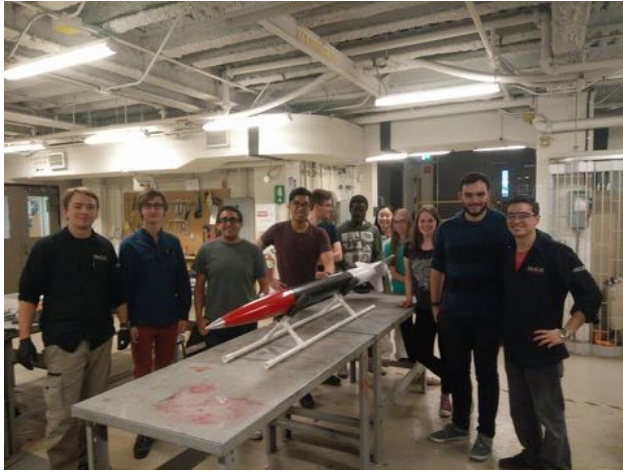
Finally, the COTS module aboard the rocket serves as a second redundancy for parachute deployment, and a third redundancy for recovery. The AIM XTRA 2.0, by Entacore Electronics, is capable of datalogging, firing e-matches, and broadcasting flight data on 433 MHz. All avionic modules are located in a central fiberglass section of the airframe for radio-transparency. The panel cut-outs, as viewed in Figure 26, allows easy accessibility and ease of assembly. The avionics are safed with “pull-pins” until arming on the launch pad, at which point these pins are removed, and power is sent to the avionic modules.



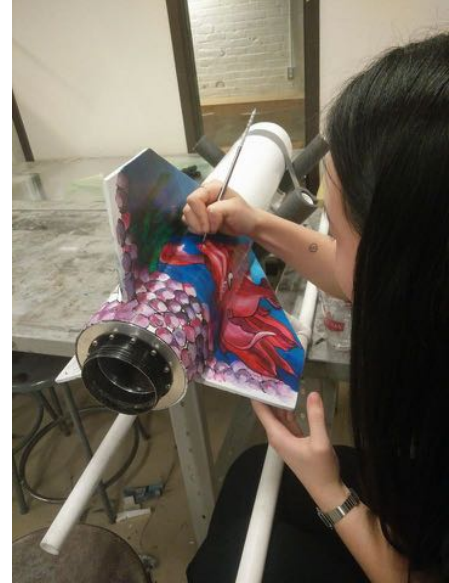
Figure 26 Avionics Bay integration with rocket.

3. Test Rocket

McGill University successfully constructed an entirely separate rocket with identical recovery and avionic systems. The rocket, named *Bertrand* after the team’s fish, was meant to fly on May 19th, 2018 but was postponed to June 2nd, 2018 due to unfavorable weather. Given that all identical systems were duplicated, the team can still afford to go to competition even if a catastrophe is experienced on this launch. However, only having an unforeseen two weeks of pivoting time limits the possible improvements that can be made to *Stella II*. Manufacturing all recovery parts in-house, along with successful sponsorship acquisition lead to massive cost savings, in-turn funding the manufacturing of the team’s third high-power rocket of the year.



(a) Launch Team after practice assembly.



(b) Friday night activities.

Figure 27 Test Rocket, *Bertrand*

D. Payload subsystems

The payload on board *Stella II* is a non-deploying scientific experiment investigating the effects of high acceleration on the human brain. The Cranial Launch Acceleration Response Experiment (C.L.A.R.E.) consists of an experimental setup to study the effects of high acceleration on the human brain in a scaled-down model. The cranium is modeled with a 3D-printed skull casing, a cerebrospinal fluid substitute, and a brain material. The material used for the brain is silicone, which allows for shaping into a geometry similar to a human brain. The silicone brain model can be viewed in Figure 28a and the 3D printed skull casing can be seen in Figure 28b.

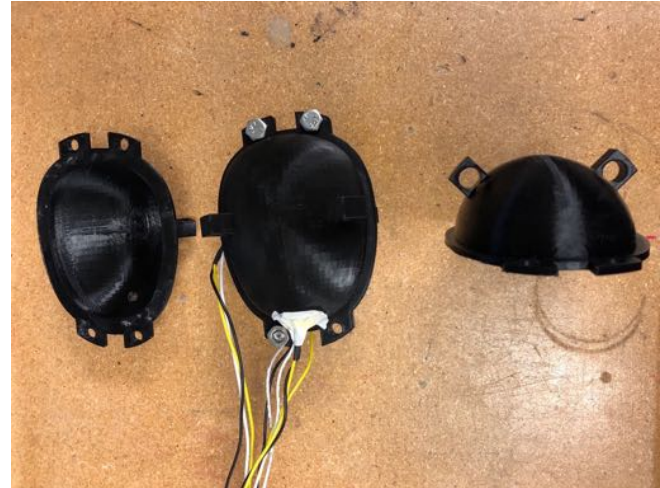
Silicone was chosen as the brain material following initial models with gelatin and agar. Though these gels hold similar mechanical properties to the brain, they did not fulfill core requirements for experiment suitability. Gelatin did not fit the melting point requirement for rocket internal temperature, melting below 40degC as measured by an infrared thermometer. Although the melting point of agar is high enough for use in the rocket, it is too brittle to withstand the expected vibrations of launch.

The forces on the brain are measured with an array of force-sensitive resistors (FSR) fixed within the simulated cranial cavity, in the cerebrospinal fluid substitute between the model skull and brain. The FSRs are arranged to reconstruct a force map on the brain, and frequent readings of force information allows force maps to be reconstructed at many points in time. The data from these FSRs is stored on a 32GB microSD card and is analyzed post flight. The whole payload is located in the nose cone, in a specialized support system meant to seamlessly integrate with the rocket while facilitating installation. A 9V, 500mAh battery is used to ensure longevity of the subsystem in case of unforeseen launch time push backs.

The brains and electronics are integrated into the rocket by means of a "Wedding cake" structure. The structure, pictured with the brains and electronics casing, is shown in Figure 30. The housing allows for easy removal and installation of the entire payload structure, while ensuring a snug connection to the rest of the rocket. The full assembly is connected directly to the nose cone's tip and integrates with the bottom plate of the nose cone. It is FEA tested to ensure that it can sustain the expected forces the nose cone will experience upon separation. At the same time, the 3D printed and sensitive skull and brain components take absolutely no direct force at any point of the launch. The brains and casings have undergone several vibration and impact tests. One of the key reasons for using silicone was to ensure that the vibrations experienced during launch do not cause the brains to lose their desired shape during data



(a) Silicone model of brain matter.



(b) Skull casing and wiring.

Figure 28 Brain Model

acquisition. Data gathering will occur during the entire duration of the mission, however the key monitoring period will be during the initial acceleration burn. Although not integral to the experiment, recovering the brain models intact would be a benefit to future work and similar modeling.

The payload housing underwent significant design within the ANSYS static structural module. A load of 1500 lbs was applied in the simulation, as an absolute worst-case scenario due to the deployment of the recovery mechanism, shown in Figure 29. This showed that the metallic components of the part could withstand a load of 3000 lbs before yield. This gives a high degree of confidence in the design of the structure.

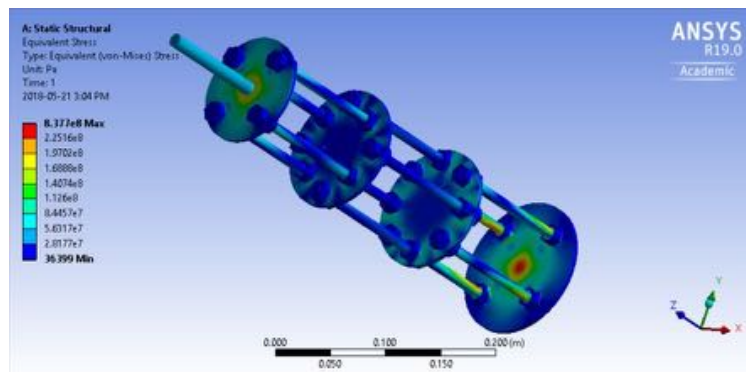


Figure 29 FEA simulation of the payload housing.



Figure 30 Payload and housing assembly.

III. Mission Concept of Operations Overview

Stella II's mission is similar to that of its predecessor. It follows a typical sounding rocket trajectory, with a single-stage burn, drogue deployment at apogee, and main chute deployment at a lower altitude. The payload is non-deploying and does not feature in the mission phases.

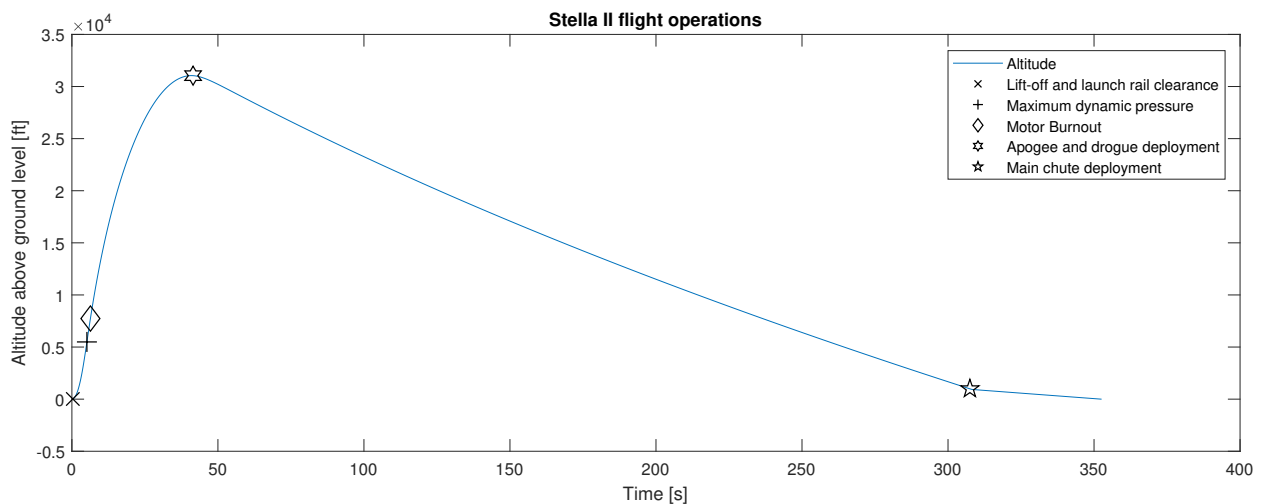


Figure 31 *Stella II* Concept of Operations

- 1) Phase 1: Pre-arming launch pad installation.
The rocket is fully assembled, with energetics circuits deactivated. Telemetry is active and transmitting to a ground station.
- 2) Phase 2: Arming.
Transition – Removing the pull pins, activating all energetics circuitry. An auditory cue is emitted by on-board buzzers. Motor igniters are inserted into the motor, secured with electrical tape and connected to the competition power supply. The ignition circuit is tested for continuity before evacuating all personnel.
- 3) Phase 3: Ignition (t = 0.00s).
Transition – Authorization is given to launch. Motor is ignited by sending a current through the igniter. The fuel grains are lit and smoke from the bottom of the rocket is visible.

- 4) Phase 4: Lift-off ($t = 0.04\text{s}$).
Transition – At first motion of rocket. Vertical motion should be observable within a few seconds of pressing of launch button. Launch rail should be cleared at $t = 0.32\text{ s}$ and at a velocity of 119 ft/s.
- 5) Phase 5: Powered ascent ($t = 0.32\text{s}$).
Transition – Upon clearing launch rail. Rocket is accelerated through thrust provided by the motor. This phase is expected to last for 6.16 seconds after takeoff. The point of maximum dynamic pressure and maximum velocity also occur in this phase, 5.14 seconds after ignition, slightly before motor burnout. No alteration to the flight path or airframe should be visible during this phase.
- 6) Phase 6: Coasting ($t = 6.16\text{s}$).
 Begins at the end of motor burn. Rocket continues its ascent to a predicted apogee of 31,047 ft.
Transition – Within moments of the rocket reaching apogee, pressure sensors detect the beginning of the descent, igniting the black powder charge well mounted on the nosecone.
- 7) Phase 7: Drogue deployment and controlled descent ($t = 40.99\text{s}$).
 The black powder combustion pressurizes the small body tube body tube section between the nosecone and the parachutes. The nosecone pops off, dragging the attached drogue chute out. Moments after being out of the body tube, the drogue inflates and slows down the descent of the rocket to 95.35 ft/s. The descent speed decreases with altitude, as air density and drag increase.
Transition – When pressure sensors detect that altitude is down to 1000 ft, the charge wells in the tender descenders are ignited.
- 8) Phase 8: Main deployment and controlled descent ($t = 307.5\text{s}$).
 Once ignited, the tender descenders separate, and the drag on the drogue chute pulls the main chute out of its bag and out of the rocket. The main inflates, and further slows the descent, to 21.29 ft/s.
Transition – The rocket eventually hits the ground, and a recovery team is dispatched with a GPS-tracking device.
- 9) Phase 9: Ground Recovery.
 The rocket is transported back for evaluation by the judges.

IV. Conclusions and Lessons Learned

2018 was a year of refinement for the team. If *Stella* was a bold venture into uncharted territory, *Stella II* is a more subtle endeavor. *Stella II's* design draws heavily from lessons learned during last year's competition. The team re-examined its design practices after both of its rockets failed to obtain a nominal flight. The team has thus prioritized improving the fundamental, basic elements of the rocket, such as the recovery system, rather than trying to experiment with new, more advanced and riskier technologies and designs. Components and subsystems were simplified wherever possible. Given the simpler design, the opportunity was taken to largely expand the inventory of SRAD components, which hugely benefited the team in many. A big lesson learned was that "simpler" does not always mean "easier," and complacency is an issue not to be taken lightly. For example;

- An overcrowded parachute chamber can muffle an ejection charge, and prevent ejection;
- A parachute-chamber which is prone to air leaks can easily lose pressure from a CO₂ ejection system, again failing ejection;
- Making square cuts on tube sections is of paramount importance, as imprecisions can cause bending moments due to non-uniform loading.

These are but a few of the oversights that the team learned (the hard way) this year. Fortunately, they were quickly addressed through experiments, but the designs of the 2018-2019 academic year will surely feature even more refined systems.

From a team management standpoint, the McGill Rocket Team experienced record-breaking member involvement and retention. This year, the team took advantage of the summer after competition to acquire as many material sponsors as possible, and get hardware delivered before the beginning of the academic year. When new recruits arrived, they were immediately thrown into a regime of heavy hands-on work. Practicing composite lay-ups, Arduino training kits, mini-launch events, and regular beers are excellent ways of maintaining a substantial, knowledgeable team that is very cohesive.

Many hours were spent in meetings coming up with the final designs presented here. Despite these simplifications, the team believes that this year's iteration is a stronger contender within the framework of the competition, and hopes to bring an enthusiasm to be reckoned with. The team is more excited for competition than ever, as McGill University brings a fantastic 29 students to the Spaceport America Cup.

References

- [1] Niskanen, S., "Development of an Open Source model rocket simulation software," *Helsinki University of Technology*, 2009.
- [2] Online, W. W., "Truth Or Consequences, New Mexico, United States of America Historical Weather Almanac," , May 2018. URL <https://www.worldweatheronline.com/truth-or-consequences-weather-history/new-mexico/us.aspx>.
- [3] Clancy, L. J., *Aerodynamics*, Halsted Press, 1975.

Acknowledgments


The team would like to acknowledge the endless support it has received from members, friends, family, donors and sponsors.

Specifically, the team would like to thank Michel Wander from the Canadian Space Agency for his advice, Yves Dufour from the Quebec Rocketry Club for lending parts and expertise, and finally all the judges and volunteers of ESRA for the countless hours spent on organizing the most exciting rocket engineering competition in the world today.

V. Appendix A - System Weights, Measures, AND Performance Data

Table 4 outlines a comprehensive list of various critical numbers that govern the design given in the 3rd progress report.


Table 4 Data from 3rd progress report.



Spaceport America Cup

Intercollegiate Rocket Engineering Competition

Entry Form & Progress Update



Color Key v18.1

SRAD – Student Researched and Designed

Must be completed accurately at all times. These fields mostly pertain to team identifying information and the highest level technical information.
Should always be completed "to the team's best knowledge", but is expected to vary with increasing accuracy / fidelity throughout the project.
May not be known until later in the project but should be completed ASAP, and must be completed accurately in the final progress report.

Date Submitted: 2017-12-07

Team ID: 93 * You will receive your Team ID after you submit your 1st project entry form.

Country: Canada

State or Province: Quebec
State or Province is for US and Canada

Team Information

Rocket/Project Name: Stella II

Student Organization Name: McGill Rocket Team

College or University Name: McGill University

Preferred Informal Name: McGill Rocket Team

Organization Type: Club/Group

Project Start Date: 2017-07-01 *Projects are not limited on how many years they take*

Category: 30k - COTS - All Propulsion Types

Member	Name	Email	Phone
Student Lead	Sandro Papis	sandro.papis@mail.mcgill.ca	514-979-2543
Alt. Student Lead	Charles Cossette	charles.cossette@mail.mcgill.ca	
Faculty Advisor	Prof. James Richard Forbes	james.richard.forbes@mcgill.ca	
Alt. Faculty Adviser			

For Mailing Awards:

Payable To:	McGill EUS - attn: McGill Rocket Team
Address Line 1:	McConnell Engineering Building, Rm 7
Address Line 2:	3480 University St.
Address Line 3:	Montreal, QC
Address Line 4:	H3A 0E9
Address Line 5:	

Demographic Data

This is all members working with your project including those not attending the event. This will help ESRA and Spaceport America promote the event and get more sponsorships and grants to help the teams and improve the event.

Number of team members

High School	0	Male	61
Undergrad	79	Female	20
Master	2	Veterans	0
PhD	1	NAR or Tripoli	0

Just a reminder the you are not required to have a NAR, Tripoli member on your team. If your country has an equivalent organization to NAR or Tripoli, you can enter them in the NAR or Tripoli box. CAR from Canada is an example.

STEM Outreach Events

We have begun organizing outreach events and a mentorship program with high schools and CEGEP colleges to help younger individuals explore their interest in rocketry to promote exposure to aerospace engineering and science. Additionally, we are looking to partner up with different engineering design teams and organizations to reach a broader audience. In particular, we held a mini rocket launch event with Vanier Cegep/College over the winter semester. This involved a presentation on general rocketry with a special focus on sounding rockets done by our team members, a building tutorial for small SRAD low powered rockets involving OpenRocket, and a launch day where the teams get to see their experiments take off. Additionally, several female members of the team attended Les Filles et les Sciences where they demonstrated some of the payloads and manufacturing that we have been working on to expand and promote young girls' interest in rocketry.

Rocket Information

Overall rocket parameters:

	Measurement	Additional Comments (Optional)
Airframe Length (inches):	132	
Airframe Diameter (inches):	5.2	
Fin-span (inches):	13.15	
Vehicle weight (pounds):	41.61	
Propellant weight (pounds):	24.09	
Payload weight (pounds):	8.85	
Liftoff weight (pounds):	74.55	
Number of stages:	1	
Strap-on Booster Cluster:	No	
Propulsion Type:	Solid	
Propulsion Manufacturer:	Commercial	
Kinetic Energy Dart:	No	

Propulsion Systems: (Stage, Manufacturer, Motor, Letter Class, Total Impulse)

1st Stage: Commercial Pro 98-60XL, 21062-03400-EM-P, O-Class, 21062.2 Ns

Total Impulse of all Motors: 21062.2 (Ns)

Predicted Flight Data and Analysis

The following stats should be calculated using rocket trajectory software or by hand.

Pro Tip: Reference the Barrowman Equations, know what they are, and know how to use them.

	Measurement	Additional Comments (Optional)
Launch Rail:	ESRA Provide Rail	
Rail Length (feet):	17	
Liftoff Thrust-Weight Ratio:	13.54	*Taken at Rail Departure
Launch Rail Departure Velocity (feet/second):	119	
Minimum Static Margin During Boost:	1.59	*Between rail departure and burnout
Maximum Acceleration (G):	15.4	
Maximum Velocity (feet/second):	1908	
Target Apogee (feet AGL):	106	
Predicted Apogee (feet AGL):	31047	

Payload Description:

The payload is functional and non-deployable, taking a non-CUBESAT form. The Cranial Launch Acceleration Response Experiment (CLARE) consists of a scientific experiment to study the effects of high acceleration on the human brain in a scaled-down model. The model will consist of a brain made of a silicone rubber material of similar mechanical properties to a living brain, in cerebrospinal fluid-like water contained within a 3D printed skull. This system will contain pressure sensors at various locations inside the cranial cavity. The purpose of the payload is to spatially and temporally localize and assess the impact of high g-force situations on the human brain. For future tests it would be possible to orient the brains differently to test for ideal human launch orientation. Each brain will contain 3 pressure sensors located on the bottom and on the sides. The symmetry of the brain will mean that we only need one sensor per side. We also do not expect the top of the brain oriented in the highest position to have a surprising amount of force as the brain will be pushed down by the acceleration and gravity and so a sensor is not present there. The electronics system for the sensors and data storage will be Arduino-based, and the data will be stored offline and retrieved from the rocket for analysis after landing.

Mounted in nose cone

Total weight: 8.8 lbs

Recovery Information

System consists of separation at the nose cone and two stage recovery
 Pressure build up results from releasing compressed CO2 in parachute chamber, breaking off shear pins at the nose cone (1st event)
 Separation deploys drogue chute as the nose cone pulls it from the parachute chamber
 An SRAD tender descender prevents the main from being pulled out at this time
 At 1000ft, a tender descender detonates, allowing the main chute to deploy (2nd event)
 The system contains two tender descenders in series to add a redundancy
 Two CO2 cannisters are in place to add redundancy, initial calculations show that one provides enough pressure to break the shear pins with a FOS of 2. Should it fail, the second cannister should provide the pressure required to eject the nose cone.

- Recovery avionics feature 4 independent systems:
- An SRAD barometer-based flight computer for ejection charge firing.
 - An SRAD telemetry and diagnostics computer, transmitting GPS coordinates and other diagnostics via 900 Mhz serial.
 - An SRAD "Morse Beacon" using a yagi antenna for short-range direction finding.
 - A COTS redundant telemetry, ejection, and diagnostics system. Specially the AIM XTRA 2.0

Planned Tests

* Please keep brief

Date	Type	Description	Status	Comments
2-15-18	Ground	Parachute Test	Successful	Drop tests
3-31-18	Ground	CO2 Mechanism Test	Successful	Successful CO2 Release
4-15-18	Ground	Recovery Avionics Test	Successful	Vacuum chamber test successful
5-10-18	In-Flight	Small Scale Flight Test	TBD	Postponed to June 2nd
4-1-18	Ground	Payload Test	Successful	Test sensor data collection in skull model
3-18-18	Ground	Tender Descender drop tests	Successful	Dynamic shock test for ejection, weights attached
4-15-18	Ground	Nose cone ejection tests	Successful	
3-24-18	Ground	Radio range and interference tests	Minor Issues	late range, modifications will be made before comp
2-1-18	Ground	Vacuum chamber avionics tests	Successful	Check logic and programming of avionics.
3-30-18	Ground	Airframe structural compression tests	Successful	Axial compression of body tubes
5-15-18	Ground	Battery life test	Successful	Verify avionics battery duration

Any other pertinent information:

General Updates:

After reviewing the feedback sent by ESRA after the first progress report, several changes were implemented into Stella II. One of the most prominent issue seen was that the stability was 0.9 cal off the rod, which was well below the required amount of 1.5 cal outlined in Section 8.3 of the design guide. This was remedied by altering the fin dimensions as necessary, and the stability off the rod has now been tuned to 1.57, complying with regulations. Additionally, in compliance with Section 8.4 of the design guide, Stella II never exceeds a stability of 6 cal, with a maximum stability of 5.56 cal. The workshop of McGill is experiencing a delay due to equipment malfunctions. While this has pushed the delivery of some components to April, and ultimately some testing, there are no concerns that the team will be unable to deliver the required testing for IREC.

Aerostructures Updates:

The composite SRAD airframe nears completion. Most of the components are manufactured and within acceptable tolerances considering the manufacturing conducted, falling within ± 0.01 in. of the target dimension. There is no reason currently to believe that this airframe is anything short of overdesigned. Compression testing of body tube samples will permit a more accurate measurement of the material properties. Current calculations are based on manufacturer data, however, due to the difficult nature of processing composites, the most accurate method of verifying performance is to test a physical sample of the product.

As a method of increasing resistance to bending moments, the coupling pieces, which are also SRAD composites manufactured in the same style as the body tubes, extend 7 in. into the various body tube sections. The produced coupling pieces fit snugly into the body tubes, and show minimal misalignment. Additionally, the components produced show excellent consistency between parts. Each 48 in. carbon fibre body tube weighs 4.3 lbs. ± 0.1 lbs. The consistent quality produced with SRAD manufacturing methodology provides further confidence in the construction of the airframe.

The last component in need of manufacturing is the carbon fibre fins. This component features a through the wall design not previously employed by the McGill Rocket Team. A makeshift resin transfer moulding process is currently being tested to ensure the resin can properly impregnate the fibres. Should this processing technique succeed, the manufacturing of this final component will take place immediately. Due to the limited resources of McGill for composite machining, several jigs are in development to make accurate cuts. These include panels in the avionics bay, slots in the body tubes for fins, and templates for the fins themselves. Proper safety considerations are being taken during this procedure, and there is a high degree of confidence in the teams ability to accurately produce the components.

To prevent the engine ripping through the airframe, a two part SRAD engine retaining system is designed. Each part of the system gives a safety factor of 2 while under loading from the peak thrust of the motor. This system is verified using ANSYS FEA, where mesh convergence has been achieved. In accordance with section 6.3 of the design guide, a glass fibre body tube and glass fibre av bay are in place directly above the engine. This provides 16" of exposed glass fibre for SRAD avionics systems, and ESRA early detection systems. After clarifying with ESRA, the use of a single detection system is considered fit, and hence glass fibre areas near the payload in the nosecone are non-existent.

Recovery Updates:

The initial testing of SRAD parachutes proceeded with favourable results. The descent rate achieved appears to be in line with expectations.

Currently, the main parachute undergoes manufacturing, and the final processing of data for the acceleration and drag coefficients is underway. The recovery mechanism, due to fears that there may be insufficient oxygen to light significant amounts of black powder at 34,000ft (not AGL) now consists of a SRAD CO2 ejection mechanism. Due to delays at the machining facilities at McGill, this device won't be produced until the end of March. Testing of the nosecone ejection will take place immediately after the receipt of these parts.

Payload Updates:

To limit the length of the rocket, the payload is now incorporated into a non-CUBESAT structure within the nose cone of the rocket. Working with the Aerostructures subteam, the housing was developed to sustain the shock caused by the deployment of the nosecone. Final analysis is being completed, but the housing appears to be rated to 2500lbs of force before failure. Once again, manufacturing of this is set to be completed by the end of March. The brain mechanism design has also been finalized. Manufacturing of the skull casing is set to finish in mid-March with the final brains moulded, and electronics tested by mid-April.

Avionics Updates:

All avionic systems have passed successful breadboard prototype tests. PCB models are being finalized and sent for manufacturing by end of March.

VI. Appendix B - Project Test Reports

A summary and list of tests performed in the 2017-2018 academic year is outlined in Table 5. Accompanying descriptions and figures can be viewed in Section II.C of this report.

Table 5 Outline of Tests 2017-2018

Subsystem	Description	Result
Recovery	Tender-Descender functionality test. Attach weights to device until separation is achieved.	35lbs required for separation.
Recovery	Tender-Descender functionality test. Simply close device and force separation with black powder charge.	Success
Recovery	CO2 Release device functionality test. Attempt release of CO2 from cannister in controlled fashion.	Success
Avionics	Ejection Circuit functionality test. Board is inserted into a vacuum chamber. Pressure is controlled to simulate flight.	Success
Avionics	Ejection Circuit functionality test. Test-launch of rocket with ejection circuit	Pending Launch - June 2nd 2018
Avionics	Battery-life tests. Boards are activated with a full battery, and left idle till deactivation.	Success - Premature termination of test after 8 hours.
Avionics	Telemetry Test. Establish functioning telemetry within airframe enclosure.	Success
Avionics	Telemetry range test. Create distance between transmitter and receiver to test range.	Failed - Insufficient range, requires a small hardware modification.
Avionics	Radio Interference test. Simultaneous transmission of 3 on-board frequencies, test for data integrity	Success
Recovery	Parachute functionality test. Drop test, check for inflation and examine descent rate with altimeter	Success - with sensor issues
Recovery	Ejection test. Eject the nose cone with empty parachute chamber.	Success
Recovery	Ejection test. Eject the nose cone with full parachute chamber	Success
Recovery	Full deployment sequence test. Verify nose cone ejection, successful drogue deployment, successful main parachute retention, successful main parachute deployment w/ tender descenders	Success
Aero-structure	Material strength test. Compressive strength of body tube sample	Success - over 21,000 lbs of force before failure.

As can be seen in Table 2, obtaining successful deployment required even more trials, along with minor modifications to the charge well locations. An over-packed parachute chamber was found to muffle ejection charges, and hence a spacer was added to create a small distance between parachute contents and the charge wells.

VII. Appendix C - Hazard Analysis

Table 6 Hazard analysis of on-board volatile materials

Hazardous Material	Storage	Handling	Transportation	Risk of Mishap and Rationale	Mitigation (Process/Design)	Risk of Injury after Mitigation
Black Powder	Stored in a dry lockable cabinet, away from flammable substances and sources of ignition	When used for testing avoid impact, friction, heat, sparks and open flame. Use instruments to measure and load, don't touch directly.	Kept in a box surrounded by padding to prevent vibration or jolts while driving.	Low	Restricted access to select individuals on the team with experience and care. Relieved at competition on site.	Very Low
Fuel Grains	Ensure it is kept cool away from direct sunlight, heat, sparks, friction, and impact.	Gently carry and install into vehicle, with care not to cause any impact.	Secured in a Nanuk foam lined container during transportation to prevent unwanted impacts or vibrations.	Low	Restricted access to select individuals on the team with experience and care. Relieved at competition on site.	Very Low
LiPo Batteries	Cool, dry areas	Avoid heat and flammable substances. Leave no exposed leads to batteries	Store in Nanuk Opaque cases for long range transportation.	Low	Careful manipulation, taking caution to not create a short-circuit. Proper storage and avoiding sources of heat.	Very Low
E-Matches	Stored in a dry lockable cabinet away from black powder, or any other flammable substances.	Careful when handling to ensure circuitry doesn't prematurely detonate.	Transported in a separate container from other potential flammables or combustibles.	Low	Restricted access to select individuals on the team with experience and care. Relieved at competition on site.	Very Low
Compressed CO2	Cool, dry areas, away from heat sources	Handle with care, avoid impacts, point nozzle away from personnel	Kept in a tight container where individual containers are constricted from movement and temperatures are not high.	Very Low	Avionics' arming procedure prevents premature puncturing of CO2 cannister.	Very Low

[H]

VIII. Appendix D - Risk Assessment

Table 7 Risk assessment of potential hazards

Hazard	Possible Causes	Risk of Mishap and Rationale	Mitigation Approach	Risk of Injury after Mitigation	Overseeing Division	Mission Phase
Explosion of solid-propellant rocket motor during launch with blast or flying debris causing injury	Cracks in propellant grain Debonding of propellant from wall Gaps between propellant sections and/or nozzle Clunk of propellant breaking off and plugging nozzle Motor case unable to contain normal operating pressure Motor end closures fail to hold	Low	Pressure test motor case (with end closures) to 1.5 maximum expected operating pressure Visually inspect motor grain for cracks, debonds, and gaps during and after assembly Use ductile (non-fragmenting) material for motor case Inspect motor case for damage during final assembly before launch Only essential personnel in launch crew Launch crew 200 feet from rocket at launch, behind barrier (vehicle)	Low	Propulsion	Phase 4 - Lift off Phase 5 - Powered ascent
Rocket deviates from nominal flight path, comes in contact with personnel at high speed	One or more fins broke off Rocket becomes aerodynamically unstable, weathercocking Body tube shatters	Medium	Simulate fins at critical points in flight, use U-G method to calculate flutter and divergence velocities Proper simulation and analysis to guarantee stability. Physical measurement of CG to validate simulation. Precision manufacturing to further validate assumptions made in simulation. Test carbon fibre samples, apply loads to test sections of body tube, complete FEA	Low	Aerostructures	Phase 5 - Powered Ascent Phase 6 - Coasting Phase
Recovery system fails to deploy, rocket or payload comes in contact with personnel	Electronics fail.	Low; several built in redundancies.	Testing of primary systems for reliability, in addition to redundant stratologgers and independent battery sources.	Low	Avionics	Phase 6 - Coasting Phase
	Pyrotechnic separation fails.	Low; tested for reliability.	Excess black powder for high safety factor of over 2, ensures separation even if 50% of black powder is not ignited.	Low		
Recovery system partially deploys, rocket or payload comes in contact with personnel	Parachutes get tangled.	Medium; orientation can be unpredictable in flight.	Professionally packed parachutes to ensure proper deployment. Clear exit paths for parachute to open fully.	Low	Recovery	Phase 7 - Drogue Deployment Phase 8 - Main Deployment

Main parachute deploys at or near apogee, rocket or payload drifts to highway(s)	Incorrect wiring, accidental electrical contacts due to acceleration and vibrations, failure of a tender descender	Medium; nature of coding/wiring is prone to mistakes	Repeated software testing, proper cable management, labeling, and repeated checks for wiring.	Low	Avionics	Phase 6 - Coasting Phase
Rocket does not ignite when command is given ("hang fire"), but does ignite when team approaches to troubleshoot	Delayed burn due to improper ignitor set up	Low; ignitors are very effective	Properly set up ignitor. If "hang fire" occurs, wait a sufficient amount of time before approaching	Low	Propulsion	Phase 3 - Ignition
Rocket falls from launch rail during prelaunch preparations, causing injury	Launch lugs break off	Low; launch lugs will be sufficiently secured.	Thread-lock used for higher strength.	Low	Aerostructures	Phase 1 - Installation
Premature engine ignition	Sparks, embers (smoking), improper grounding for igniter	Low; engine will be handled with care	Prevent any ignition sources to be near unpacked fuel grains. Follow the engine igniter procedures for on-rail installation, and re-explained by IREC officials.	Low	Propulsion	Phase 1 - Installation; Phase 2 - Arming
Grain blowout (casing related)	Improper engine casing assembly	Low; assemble with care	Follow manufacturer instructions and tips from last year's team.	Low	Propulsion	Phase 1 - Installation
Power Loss	Batteries not fully charged. Severed wires due to high acceleration.	Low	Batteries of excessive battery life are used, and are charged the night before whilst under proper storage conditions.	Low	Avionics	All phases past Phase 2 - Arming
Failure To Detonate At Decoupling Event Altitude	Power Loss, wire severance due to high acceleration speeds, bad e-match	Medium	Redundant systems that are entirely independent with alternative apogee detection schemes	Low	Avionics	Phase 6 - Coasting Phase

Loss of Flight Data	Loss of communication with rocket.	Medium	Data is logged to internal memory of GPS module. Memory is independently powered.	Low	Avionics	Phase 7 - Drogue Descent, Phase 8 - Main Descent
Loss Of Communication With Rocket	Electromagnetic interference, power issues, radio interference, lack of radio transparency.	High	Full triple-redundant position is broadcasted to ground station via three different frequencies. Use of radio-transparent materials and non-conductive housing prevents radio interference. Directional antennas used for signal amplification.	Low	Avionics	All phases past Phase 2 - Arming
Loss Of Rocket Position	Sensor failure, communication failure, catastrophic event.	High	Triple redundant telemetry, rigorous airframe design and manufacture, use of COTS telemetry for enhanced reliability.	Low	Avionics	All phases past Phase 2 - Arming
Failure to deploy payload	Jamming within parachute chamber, prevents main deployment.	Medium	Drogue parachute inflation occurs earlier in recovery sequence, hence applies a force on the payload for deployment.	Low	Payload	Phase 7 - Drogue Descent

IX. Appendix E - Assembly, Pre-flight, Launch Checklists

Table 8 Operations checklist for *Stella II*

MRT Operations Checklist

Project Stella II		June 2018	
Step	Division	Task	Complete
ASSEMBLE RECOVERY SYSTEMS			
1.0	Recovery	Pack main parachute in deployment bag	<input type="checkbox"/>
1.1	Structure	Fold drogue and wrap in nomex blanket	<input type="checkbox"/>
1.2	Structure	Weigh black powder, add to Tender Descender Mechanism mechanism, and close TD with set screw	<input type="checkbox"/>
1.3	Structure	Connect all shock chords as per diagram.	<input type="checkbox"/>
ASSEMBLE AVIONICS BAY			
2.0	Avionics	Make sure main power switches are turned off.	<input type="checkbox"/>
2.1	Avionics	Visually verify all main power connections	<input type="checkbox"/>
2.2	Avionics	Slide body tube section over avionics bay	<input type="checkbox"/>
2.3	Avionics	Screw body tube section into place	<input type="checkbox"/>
2.4	Avionics	Insert circuit-breaker pins	<input type="checkbox"/>
2.5	Avionics	Connect e-matches to screw terminals	<input type="checkbox"/>
2.6	Avionics	Activate main power switch	<input type="checkbox"/>
2.7	Avionics	Wait till rocket is on launch pad to arm.	<input type="checkbox"/>
ASSEMBLE NOSE CONE ENCLOSURE			
3.0	Payload	Activate payload electronics.	<input type="checkbox"/>
3.1	Payload	Insert payload "wedding cake" assembly into nose cone.	<input type="checkbox"/>
3.2	Structure	Screw nose-cone tip onto protruding threaded rod.	<input type="checkbox"/>
3.3	Structure	Ensure nose cone assembly integrity is sufficiently tight/robust.	<input type="checkbox"/>
3.4	Structure	Attach drogue shock cord to nose cone u-bolt.	<input type="checkbox"/>
ASSEMBLY UPPER BODY TUBE			
4.0	Structure	Attach shock cord to parachute bag, include swivels	<input type="checkbox"/>
4.1	Structure	Attach upper body tube to av coupler	<input type="checkbox"/>
4.2	Structure	Attach shock cords to nose cone and AV bay eyebolts using quick links.	<input type="checkbox"/>
4.3	Avionics	Verify functioning telemetry	<input type="checkbox"/>
4.4	Structure	Insert Parachutes, AV bay and Nose cone into body tube.	<input type="checkbox"/>
4.5	Structure	Insert AV-Body tube screws	<input type="checkbox"/>
4.6	Structure	Insert four shear pins.	<input type="checkbox"/>

ASSEMBLE LOWER BODY TUBE

5.0 Propulsion	Obtain motor, spacer, e-matches from vendor and verify components	<input type="checkbox"/>
5.1 Propulsion	Grease motor casing and threads on motor casing with silicone spray	<input type="checkbox"/>
5.2 Propulsion	Assemble motor as per manufacturer instructions	<input type="checkbox"/>
5.3 Propulsion	Insert engine into rocket	<input type="checkbox"/>
5.4 Structure	Screw motor retainer cap	<input type="checkbox"/>

FINAL ROCKET ASSEMBLY

6.0 Structure	Attach long shock cord to main parachute	<input type="checkbox"/>
6.1 Structure	Place nomex blanket for drogue/payload	<input type="checkbox"/>
6.2 Structure	Z fold extra long shock cord	<input type="checkbox"/>
6.3 Structure	Screw body tube sections into corresponding coupling pieces	<input type="checkbox"/>
6.4 Avionics	Verify functioning telemetry	<input type="checkbox"/>

PREFLIGHT CHECKLIST

Nominal Procedure

7.0 N/A	Carry rocket out to launch pad	<input type="checkbox"/>
7.1 N/A	Install rocket on rail	<input type="checkbox"/>
7.2 N/A	Set launch angle on rail	<input type="checkbox"/>
7.3 Avionics	Arm - remove pull-pins	<input type="checkbox"/>
7.4 Avionics	Ensure proper beep sequence and active telemetry	<input type="checkbox"/>
7.5 Propulsion	Install engine igniter	<input type="checkbox"/>
7.6 Propulsion	Verify continuity on motor igniter	<input type="checkbox"/>

Off-nominal Procedure

Propulsion	Remove engine igniter	<input type="checkbox"/>
N/A	Disarm - re-insert circuit-breaker pins	<input type="checkbox"/>
N/A	Remove rocket from launch rail	<input type="checkbox"/>

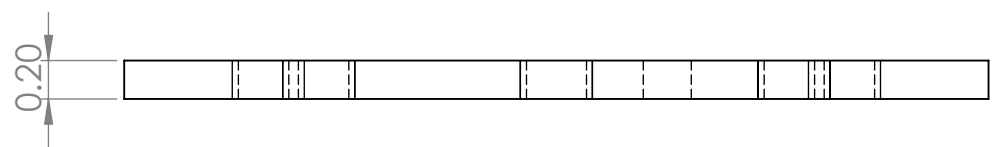
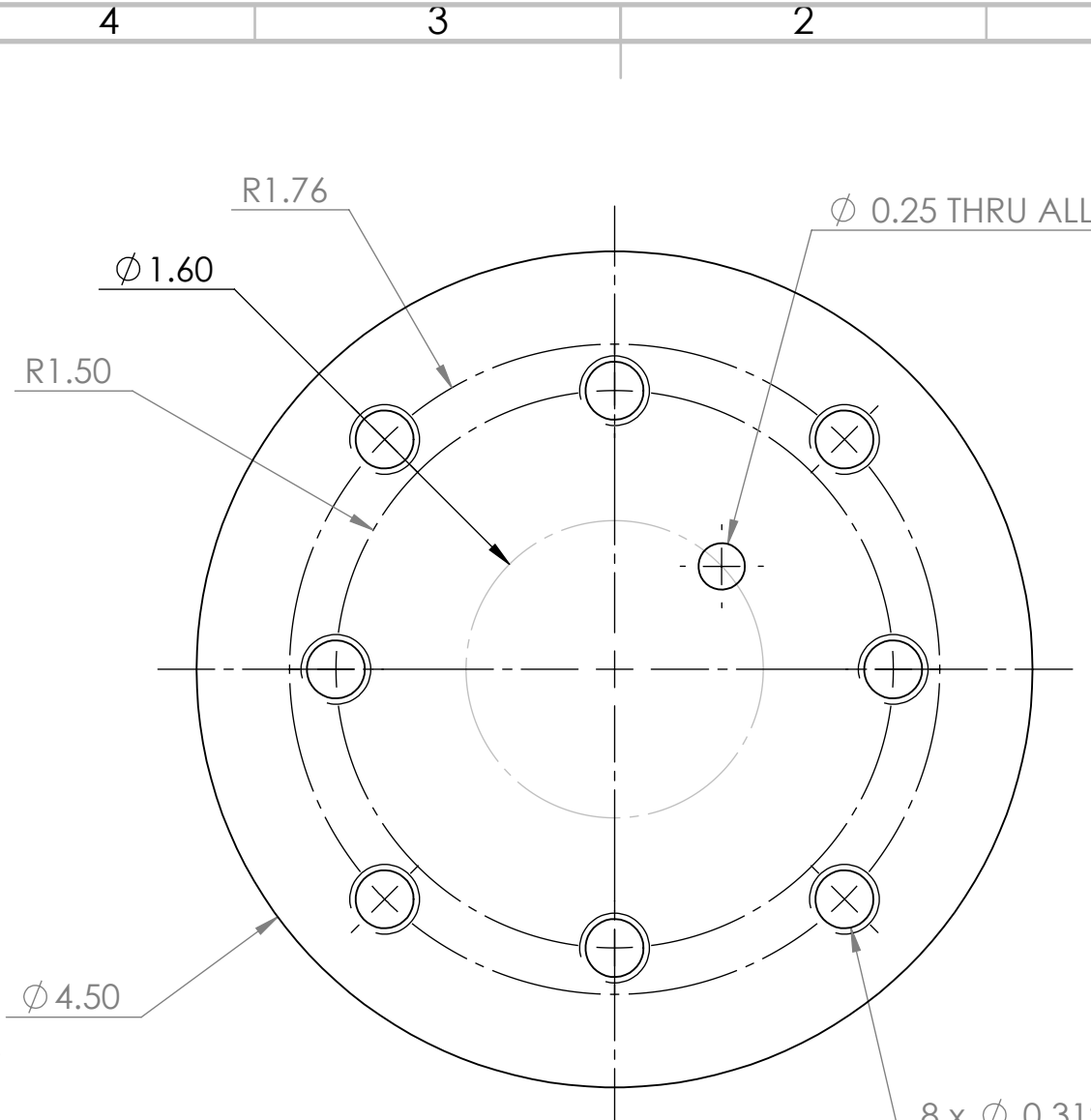
LAUNCH CHECKLIST

- | | | |
|----------------|---|--------------------------|
| 8.0 | Nominal Procedure | |
| 8.1 Propulsion | ignite motor | <input type="checkbox"/> |
| 8.2 All | Track rocket through telemetry and visual aid | <input type="checkbox"/> |
| 8.3 | Off-nominal Procedure | <input type="checkbox"/> |
| 8.4 Propulsion | Remove engine igniter if still in rocket motor. | <input type="checkbox"/> |
| 8.5 All | Take cover until given all clear to approach rocket or rocket wreckage | <input type="checkbox"/> |
| 8.6 Avionics | insert circuit-breaker pins to cut power to all avionics connected to energetics. | <input type="checkbox"/> |

RECOVERY CHECKLIST

- | | | |
|--------------|--|--------------------------|
| 9.0 Avionics | if arming lock is still in tact and it is possible to do so, disarm - insert circuit-breaker pin and deactivate switch to disengage all electronics. | <input type="checkbox"/> |
| 9.1 All | Recover all sections of rocket and any pieces that may have broken off. | <input type="checkbox"/> |

X. Appendix F - Engineering Drawings



UNLESS OTHERWISE SPECIFIED:
 DIMENSIONS ARE IN INCHES
 SURFACE FINISH:
 TOLERANCES:
 LINEAR:
 ANGULAR:

FINISH:

DEBURR AND
 BREAK SHARP
 EDGES

DO NOT SCALE DRAWING

REVISION

McGill Rocket Team

TITLE:
MIDDLE PLATE V2

	NAME	SIGNATURE	DATE
DRAWN			
CHK'D			
APPV'D			
MFG			
Q.A			

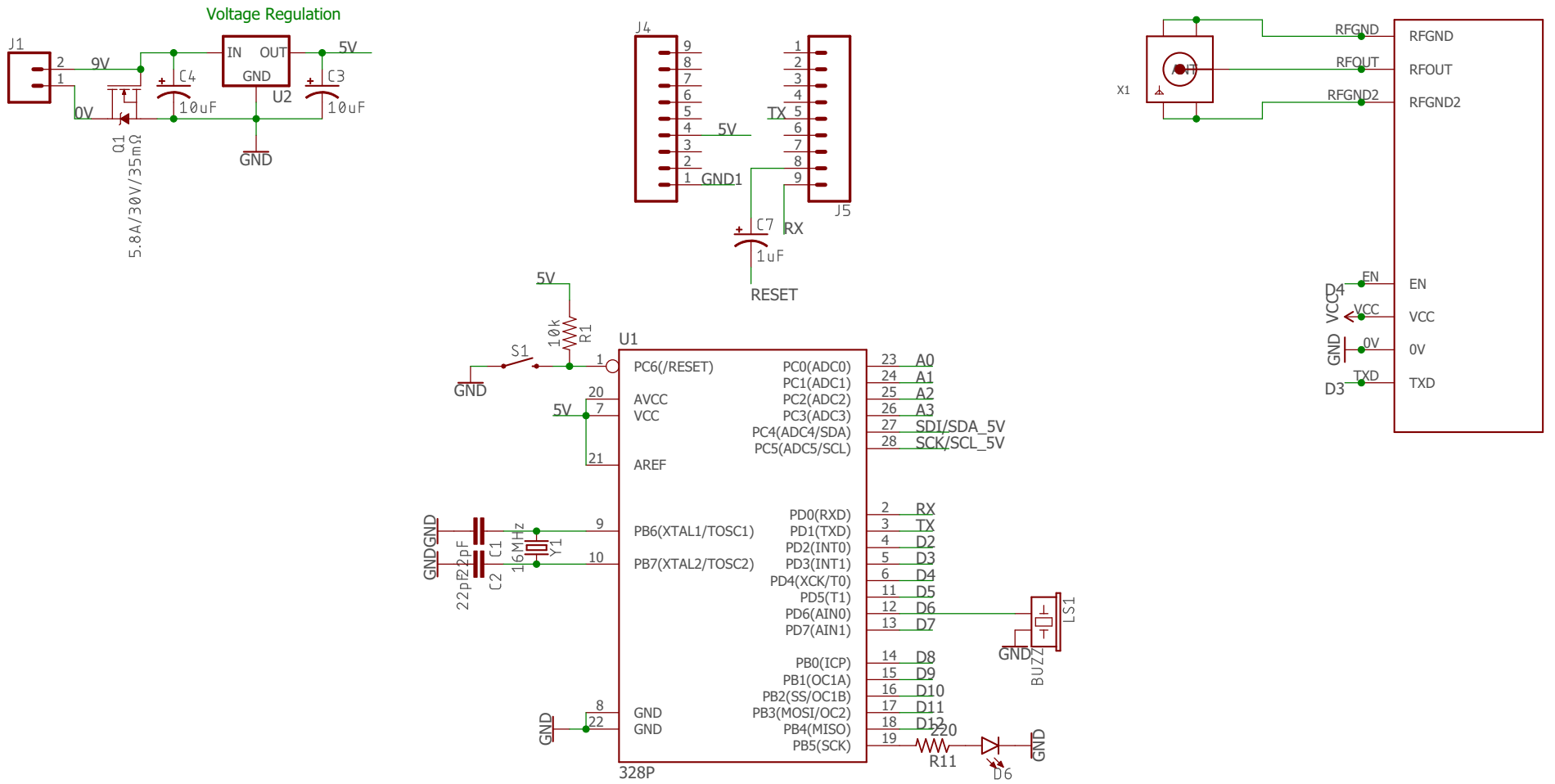
DWG NO. Middle_Plate_V2_Drawing

A4

WEIGHT:

SCALE:1:1

SHEET 1 OF 1



Released under the Creative Commons Attribution Share-Alike 4.0 License
<https://creativecommons.org/licenses/by-sa/4.0/>

TITLE: Morse_Beacon_PTH_2018

Design by: **Charles Cossette**
 514-668-2195

REV: **1**

Date: 2018-03-17 5:13 PM

Sheet: 1/1

6

5

4

3

2

1

8 x #8-32 Tapped Hole

.625±.010

.78

.33

Ø 3.92

Ø 4.985±.005

Ø 4.625±.010

Ø 4.35

SECTION A-A

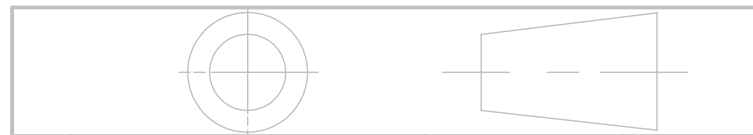
A

A

DO NOT SCALE DRAWING

REVISION

McGill University



	NAME	SIGNATURE	DATE	TITLE: Stella Bottom Retainer
DRAWN	Siddharth Raghavan		02/04/18	
APPVD	Jonathan Lesage		11/04/18	
UNLESS OTHERWISE SPECIFIED: DIMENSIONS ARE IN INCHES SURFACE FINISH: TOLERANCES: LINEAR: +/- 0.01		QUANTITY: 1	MATERIAL: Aluminium 6061 T6	DWG NO. 3
		WEIGHT: 0.4 lbs	SCALE: 1:2	A4

TITLE: Stella Bottom Retainer	
DWG NO. 3	A4
SCALE: 1:2	SHEET 1 OF 1

6

5

4

3

2

1

D

D

C

C

B

B

A

A

4 3 2 1

F

E

D

C

B

A

F

E

D

C

B

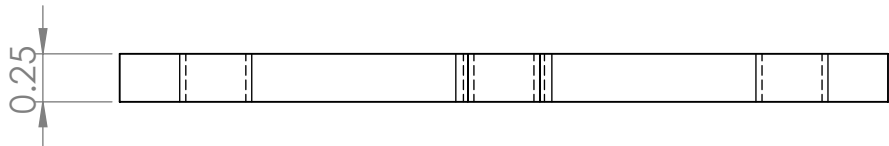
A

4 x ϕ 0.3125 THRU ALL
3/8-16 UNC THRU ALL

ϕ 0.4219 THRU ALL
1/2-13 UNC THRU ALL

ϕ 3.00

ϕ 4.00



UNLESS OTHERWISE SPECIFIED:
DIMENSIONS ARE IN INCHES
SURFACE FINISH:
TOLERANCES:
LINEAR:
ANGULAR:

FINISH:

DEBURR AND
BREAK SHARP
EDGES

DO NOT SCALE DRAWING

REVISION

McGill Rocket Team

TITLE:

TOP PLATE

	NAME	SIGNATURE	DATE
DRAWN			
CHK'D			
APPV'D			
MFG			
Q.A			

MATERIAL:

DWG NO.

Top_Plate_Drawing

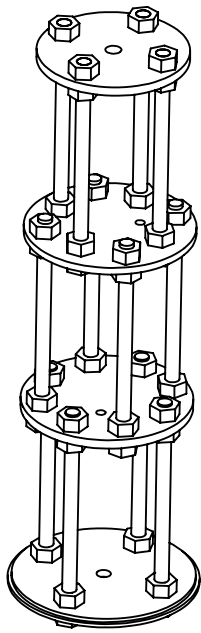
A4

WEIGHT:

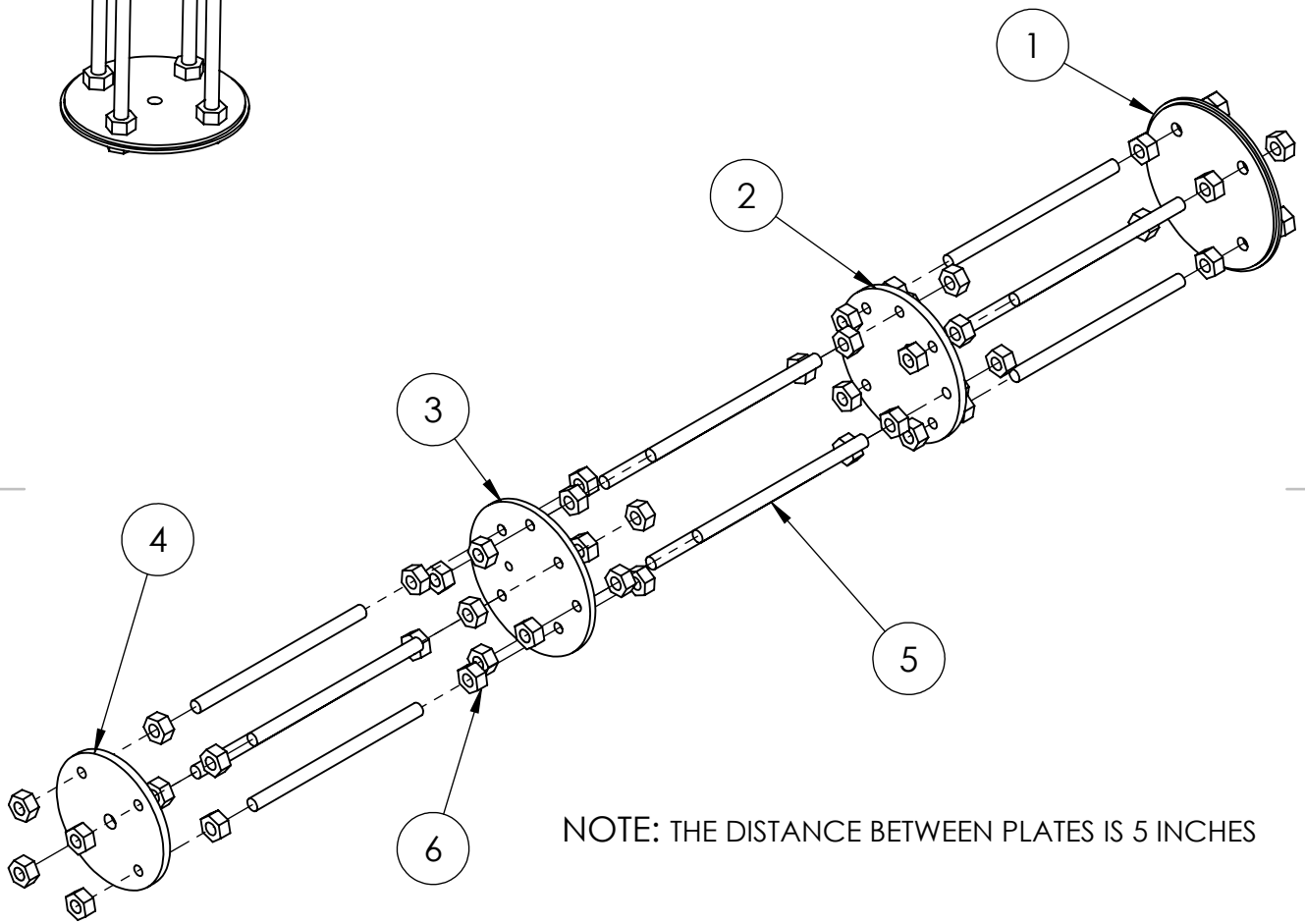
SCALE:1:1

SHEET 1 OF 1

4 3 2 1



ITEM NO.	PART NAME	DESCRIPTION	QTY.
1	Bottom_Plate	Carbon Fiber Nose Cone Lid	1
2	Middle_Plate_V1	Steel Plate	1
3	Middle_Plate_V2	Steel Plate	1
4	Top_Plate	Steel Plate	1
5	0.375_Inch_Rod	3/8-16 Rod	12
6	0.375_Inch_Nut	3/8-16 Nut	48



NOTE: THE DISTANCE BETWEEN PLATES IS 5 INCHES

UNLESS OTHERWISE SPECIFIED:
 DIMENSIONS ARE IN INCHES
 SURFACE FINISH:
 TOLERANCES:
 LINEAR:
 ANGULAR:

FINISH:

DEBURR AND
 BREAK SHARP
 EDGES

DO NOT SCALE DRAWING

REVISION

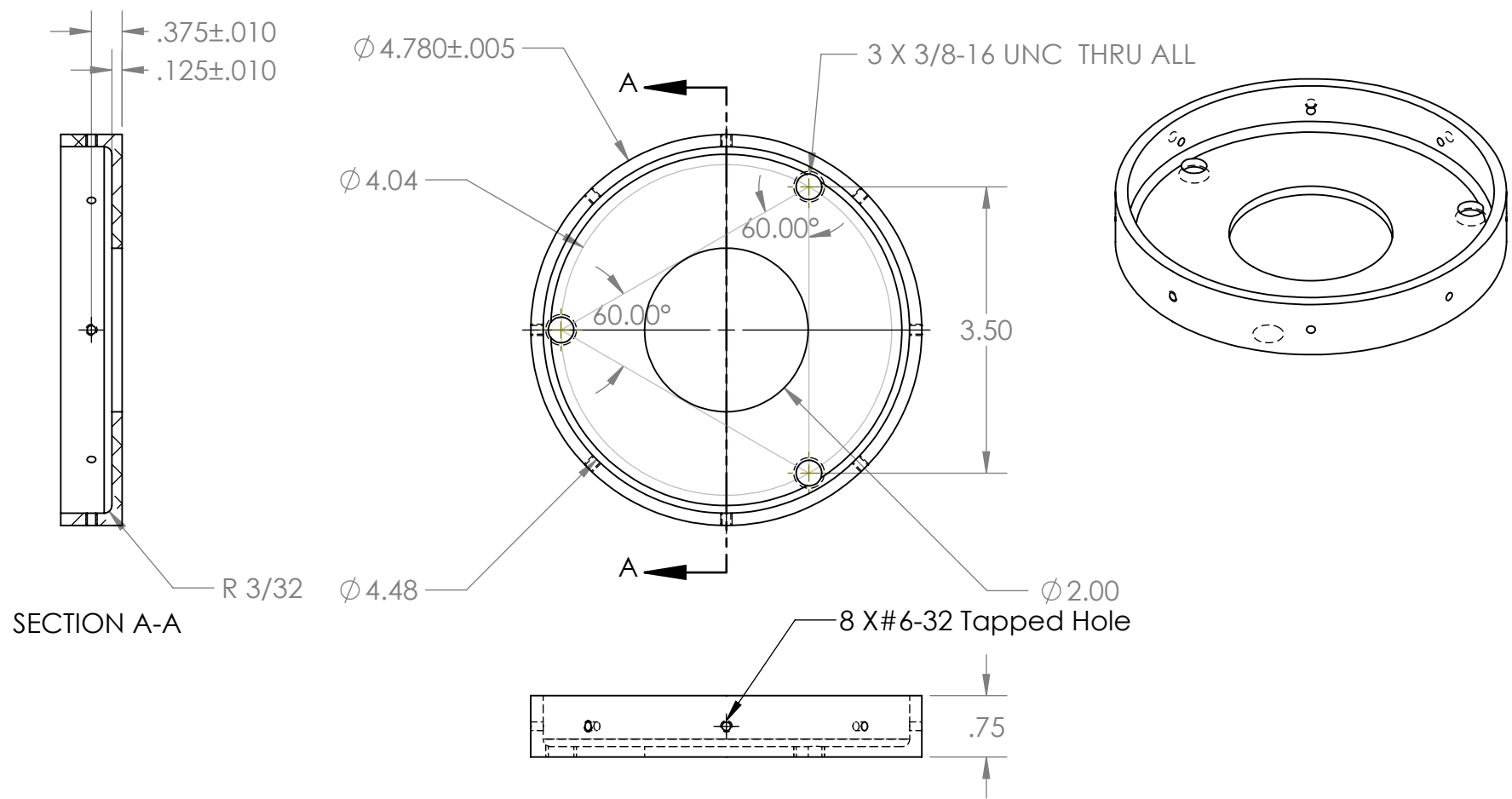
McGill Rocket Team

NAME	SIGNATURE	DATE
DRAWN		
CHK'D		
APPV'D		
MFG		
Q.A		

TITLE:	PAYLOAD INTERFACE
DWG NO.	
Wedding_Cake_Assembly_Drawing	
SCALE: 1:5	SHEET 1 OF 1

6 5 4 3 2 1

D
C
B
A



D
C
B
A

		DO NOT SCALE DRAWING		REVISION	
		McGill Rocket Team			
NAME		SIGNATURE		DATE	
DRAWN: Siddharth Raghavan				02/04/18	
APPVD: Jonathan Lesage				11/04/18	
UNLESS OTHERWISE SPECIFIED: DIMENSIONS ARE IN INCHES SURFACE FINISH: TOLERANCES: LINEAR: +/- .001		QUANTITY:		TITLE: Engine Top Retainer	
		2			
		MATERIAL: Aluminium 6061 T6		DWG NO.:	
WEIGHT: 0.31 lbs		SCALE: 1:2			
				A4	
				SHEET 1 OF 1	

6

5

4

3

2

1

D

D

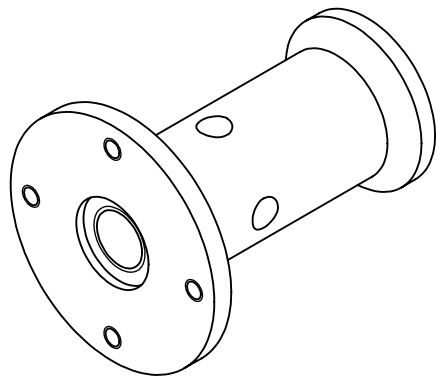
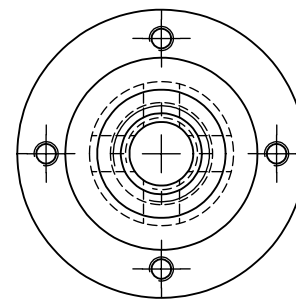
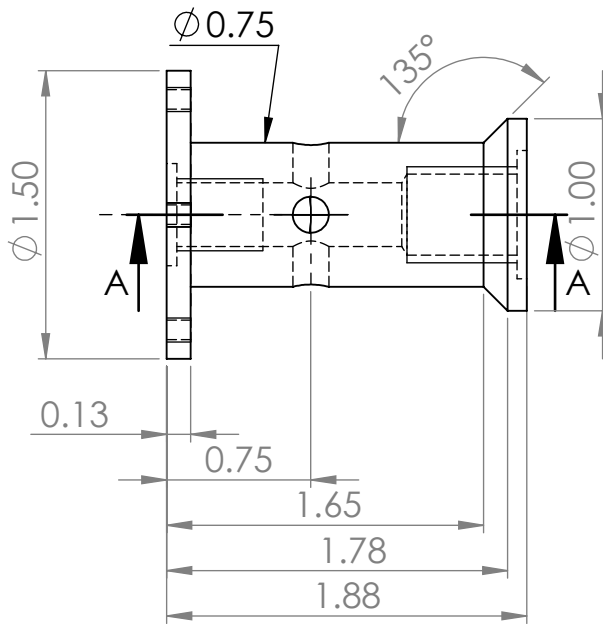
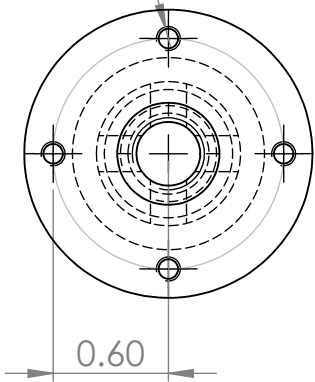
ϕ 0.33 ∇ 0.50
3/8-24 UNF ∇ 0.50

ϕ 0.19 X 4 THRU

ϕ 0.42 ∇ 0.63
1/2 UNC ∇ 0.63

SECTION A-A

4 x 5-40 UNC ∇ THRU



C

B

A

UNLESS OTHERWISE SPECIFIED:
DIMENSIONS ARE IN INCHES
TOLERANCES:
LINEAR: \pm 0.01
ANGULAR: \pm 0.5°

QUANTITY: 4

DO NOT SCALE DRAWING

REVISION 3

MCGILL UNIVERSITY

	NAME	SIGNATURE	DATE		
DRAWN					
CHK'D					
APPV'D					
MFG					
Q.A					
			MATERIAL: ALUMINUM		
			WEIGHT:		

TITLE:
BASE

DWG NO. 1 A4

SCALE: 1:1 SHEET 1 OF 1

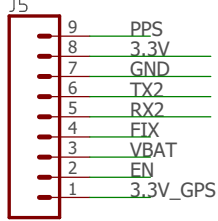
4

3

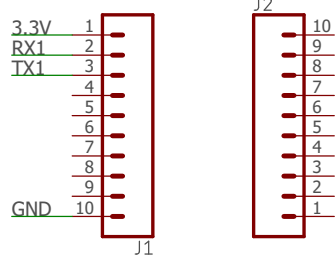
2

1

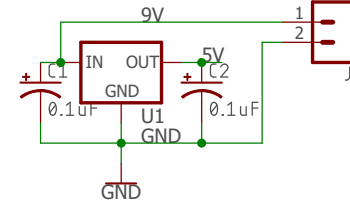
Adafruit Ultimate GPS



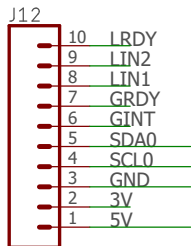
XBEE PRO 900



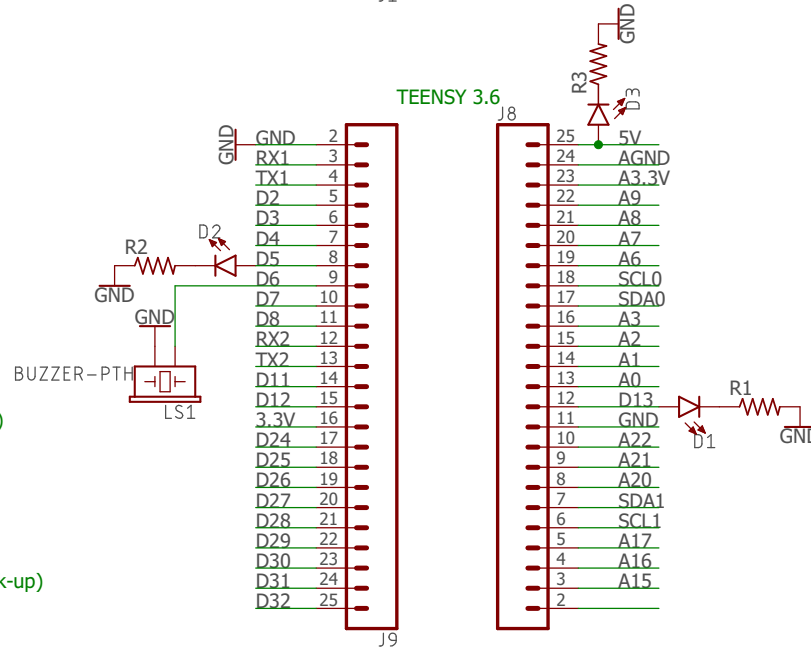
Power



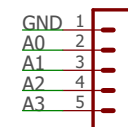
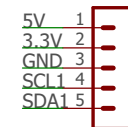
Adafruit 10 DOF IMU



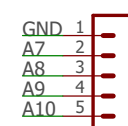
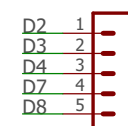
TEENSY 3.6



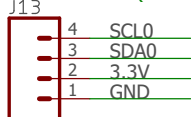
External Connections



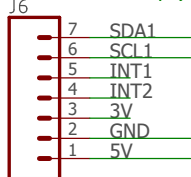
- Light Sensor
- Fin Sensor 1
- Fin Sensor 2
- Fin Sensor 3



Sparkfun 9 DOF IMU (back-up)



Adafruit Barometer and Temp (back-up)



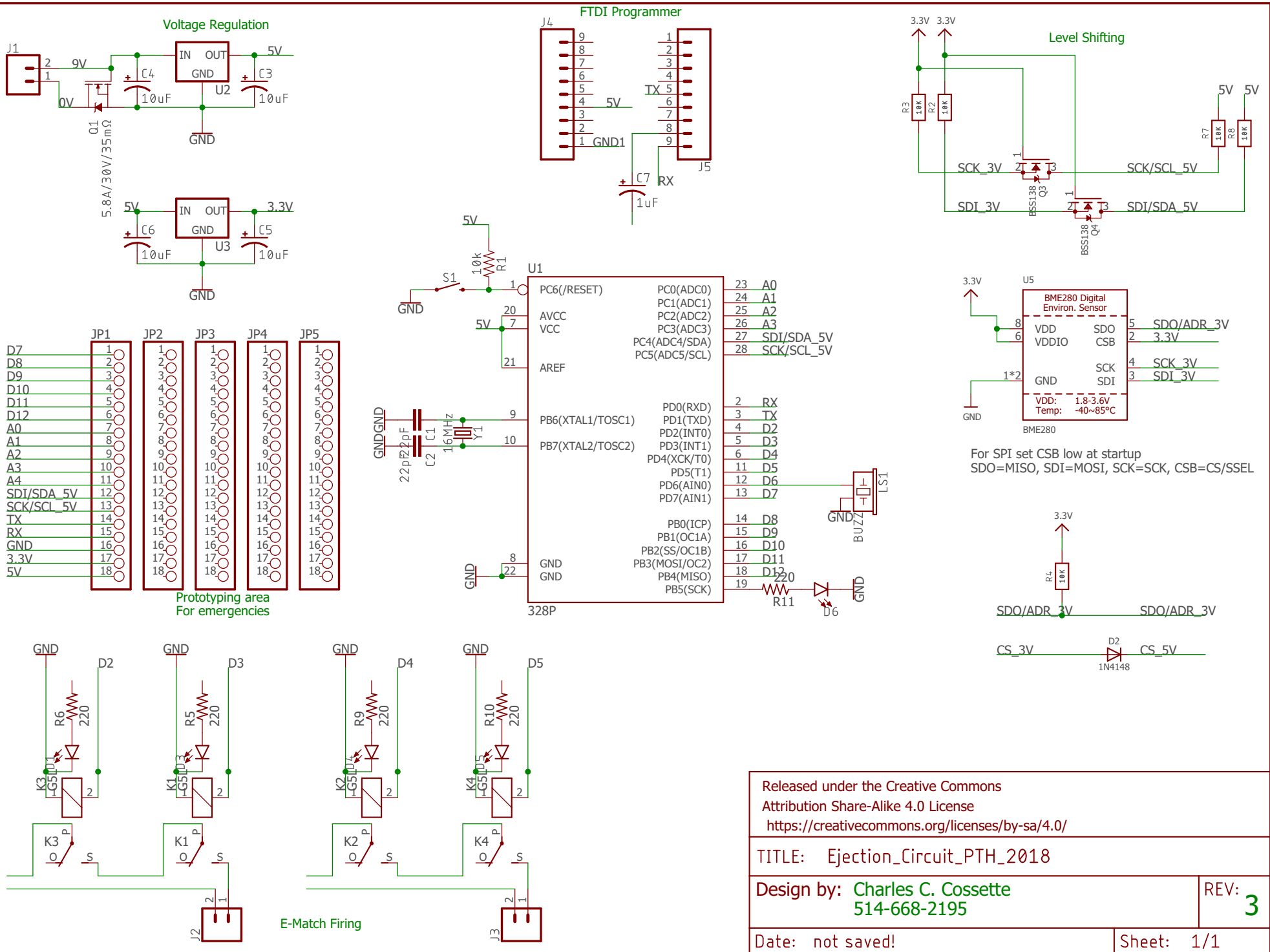
Released under the Creative Commons Attribution Share-Alike 4.0 License <https://creativecommons.org/licenses/by-sa/4.0/>

TITLE: Diagnostics_PTH_2018

Design by: _____ REV: _____

Date: 2018-03-08 5:18 PM

Sheet: 1/1



Released under the Creative Commons Attribution Share-Alike 4.0 License
<https://creativecommons.org/licenses/by-sa/4.0/>

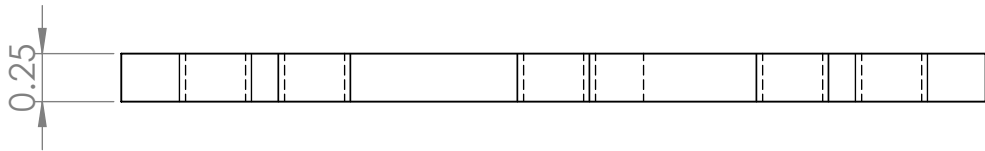
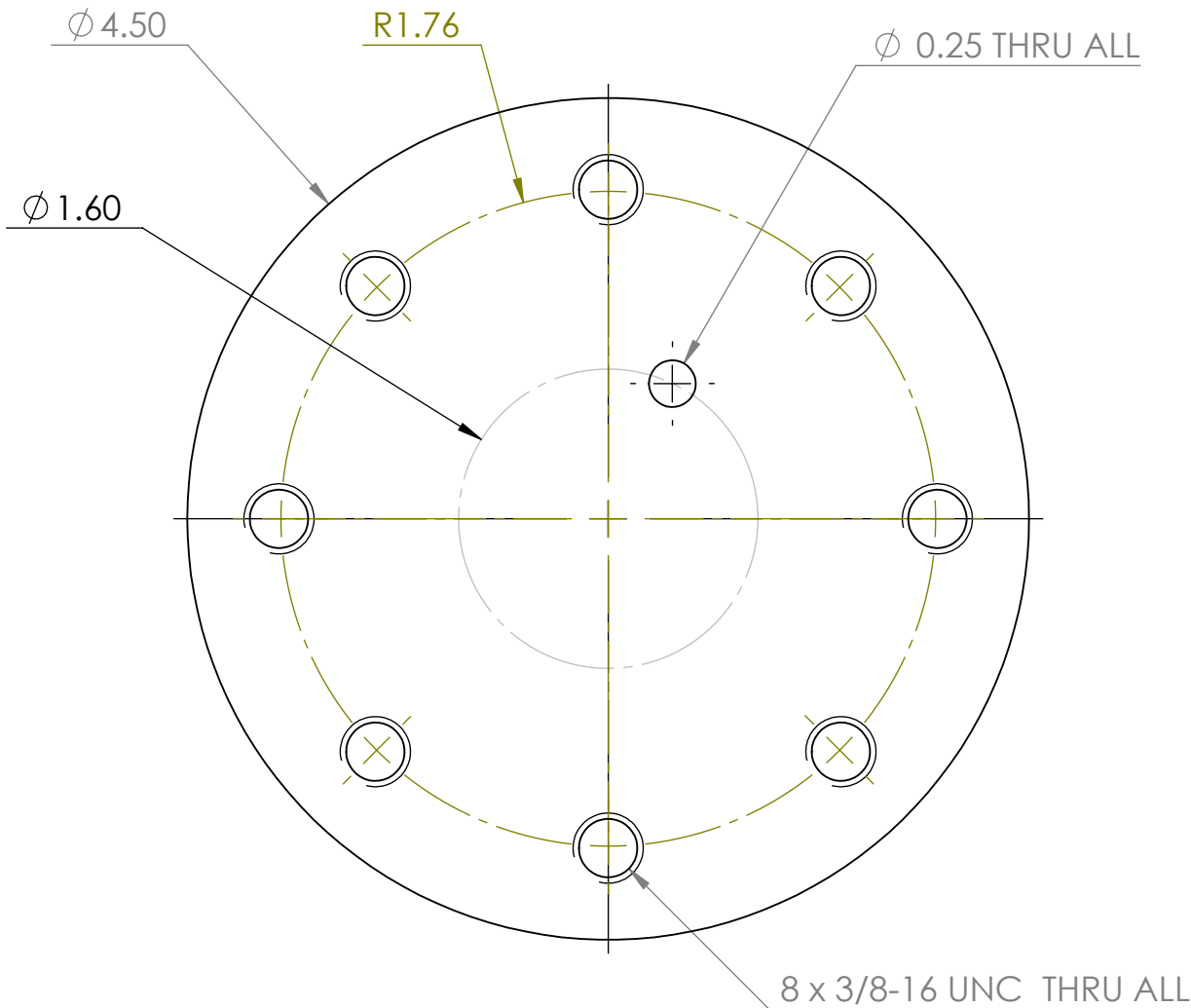
TITLE: Ejection_Circuit_PTH_2018

Design by: Charles C. Cossette
 514-668-2195

REV: 3

Date: not saved!

Sheet: 1/1



UNLESS OTHERWISE SPECIFIED:
 DIMENSIONS ARE IN INCHES
 SURFACE FINISH:
 TOLERANCES:
 LINEAR:
 ANGULAR:

FINISH:
 DEBURR AND
 BREAK SHARP
 EDGES

DO NOT SCALE DRAWING REVISION

McGill Rocket Team

TITLE:
MIDDLE PLATE V1

	NAME	SIGNATURE	DATE
DRAWN			
CHK'D			
APPV'D			
MFG			
Q.A			

MATERIAL:
STEEL
 WEIGHT:

DWG NO. Middle_Plate_V1_Drawing A4
 SCALE:1:1 SHEET 1 OF 1